J. Physiol. (1987), **394**, *pp.* 529–572
With 15 text-figures
Printed in Great Britain

KINETICS AND COMPONENTS OF THE FLASH PHOTOCURRENT OF ISOLATED RETINAL RODS OF THE LARVAL SALAMANDER, *AMBYSTOMA TIGRINUM*

BY W. H. COBBS AND E. N. PUGH JR

From the Departments of Biophysics and Psychology, University of Pennsylvania, Philadelphia, PA 19104, U.S.A.

(*Received 3 February 1987*)

SUMMARY

1. Membrane currents initiated by intense, 20 μs flashes (photocurrents) were recorded from isolated salamander rods by combined extracellular suction electrodes and intracellular tight-seal electrodes either in current or voltage clamp mode. The magnitudes (mean $\pm$2 S.E.M.) of the maximal photoresponses recorded by the suction and by the intracellular electrode respectively were 40$\pm$5 pA (n = 18) and 35$\pm$7 mV (n = 8) for current clamp at zero current; 43$\pm$9 pA and 66$\pm$13 (n = 11) pA for voltage clamp at the zero-current holding potential, $-$24$\pm$3 mV.

2. Photocurrents initiated by flashes isomerizing 0·1% or more of the outer segment's rhodopsin achieved a saturated velocity and were 95% complete in less than 50 ms. The effect of incrementing flash intensity above 0·1% isomerization can be described as a translation of the photocurrent along the time axis towards the origin. Within the interval 0–50 ms the latter two-thirds of the velocity-saturated photocurrent is well described as a single-exponential decay. The decay was much faster in voltage clamp (2·8$\pm$1·2 ms, n = 11) than in current clamp mode (17$\pm$5 ms, n = 17).

3. The initial third of the velocity-saturated photocurrent, occurring over the interval from the flash to the onset of exponential decay, followed about the same time course in current and voltage clamp. The time interval occupied by this initial 'latent' phase decreased with increasing flash intensity and attained an apparent minimum of about 7 ms in response to flashes isomerizing 10% or more of the rhodopsin at *ca.* 22 °C.

4. The hypothesis that the decay of outer segment light-sensitive membrane current is the same in current and voltage clamp was supported by an analysis of the difference between outer segment currents measured successively in the two recording modes. First, the tail of the difference current decayed exponentially with a time constant approximately equal to $R \times C$, where R and C are independently estimated slope resistance and capacitance of the rod. Secondly, the integral of the difference current, when divided by outer segment capacitance, closely approximated the hyperpolarizing light response measured under current clamp. Thus, displacement current accounted for the difference between photocurrents measured in current and voltage clamp.

5. The hypothesis that a delay stage intrinsic to phototransduction, not voltage-clamp resolution, was largely responsible for the 2·8 ms decay rate limitation measured under voltage clamp was supported by two observations. First, clamp settling time was up to 7 times faster than decay of light-sensitive current. Secondly, inner segment membrane current measured with the suction electrode was found to be negligible in a rod that gave a simultaneously measured 45 pA voltage clamp photocurrent with a 2·5 ms decay.

6. A cascade of reactions comprising sequential activation of rhodopsin, guanine nucleotide binding protein and phosphodiesterase, depletion of cyclic GMP and cyclic GMP-dependent conductance decrease, employing rate constants consistent with published biochemical data, was examined by numerical analysis and compared with the velocity- and decay-saturated voltage clamp photocurrents.

7. The theoretical analysis shows that maximal, saturated photocurrent velocity could be determined either by the rate of closure of the light-sensitive conductance or by the hydrolytic rate limitation set by the maximal phosphodiesterase activity. The latter explanation appears to be preferable by virtue of closer consistency with published rate constants of components of the cyclic GMP cascade.

8. The theoretical analysis also shows that the 7 ms minimum delay to acquisition of maximal photocurrent velocity can be explained by the cyclic GMP cascade only if about four delay steps of magnitude about 2 ms are postulated to intervene between activation of rhodopsin and phosphodiesterase.

9. In simulations that reproduce the measured velocity- and delay-saturated voltage clamp photocurrent, the entire dependence of the photocurrent on subsaturating flash intensity can be assigned to a single rate constant, governing the time course with which each photolysed rhodopsin activates a pool of guanine nucleotide binding protein. Variation of this rate constant reproduced the translation behaviour of the photocurrent measured in response to flashes isomerizing more than 0·1 % of the rhodopsin.

10. When measured over times greater than about 50 ms after an intense flash, the outer segment membrane current initiated by a saturating flash exhibited a component that was light-insensitive and that followed a relatively slow, approximately exponential time course. The amplitude of this latter current varied from 1 to 5 pA ($3{\cdot}3 \pm 1{\cdot}1$ pA, $n = 10$); the time constant varied from 0·4 to 1·4 s ($0{\cdot}70 \pm 0{\cdot}18$ pA, $n = 10$). This current, which closely resembles that previously identified in toad as the electrogenic component of an Na–Ca exchange, contributed negligibly to the current transients measured in the initial 50 ms after intense flashes.

INTRODUCTION

Observations of the kinetic behaviour of rod and cone photoresponses have been analysed in theoretical treatments in which an internal, diffusible messenger modulates the light-sensitive current. Penn & Hagins (1972), by extracellular methods in rat retina, found that whereas flash photocurrent amplitude saturated hyperbolically with half-saturation at *ca.* 30 isomerizations, the rate of rise of photocurrent increased with light intensity over about 1000-fold greater range of

intensities, reaching half-saturation at about 40000 isomerizations. These findings were found to be consistent with a theory in which light produced transmitter at an initial rate linear in the number of photolysed rhodopsin molecules. Baylor, Hodgkin & Lamb (1974), in an analysis of the intracellularly recorded photovoltages of turtle cones, similarly concluded that their observations in the first 50 ms after a flash were consistent with a theory in which light produced a conductance antagonist or 'blocking particle' at a rate proportional to the number of absorbed photons.

In the theoretical analyses of Penn & Hagins (1972) and of Baylor *et al.* (1974) no kinetic limitation intrinsic to the chain of events after photon absorption limited the rate of rise of the photoresponse: the rate of release of transmitter was predicted to increase over the entire range of flash intensities that produce increasing numbers of isomerizations. In each case, however, electrical properties of the system set a resolution limit on the measurement of the rate of rise of the photoresponse. In the intracellular recordings from turtle cones, the cell time constant of *ca.* 6 ms set the limit. In the extracellular recordings from rat retina at 34 °C the shortest time for the photocurrent to go from 20 to 80 % completion was 700 μs; this limitation was shown to be predicted by a model of passive cable propagation in the rat rod.

The two studies just discussed antedate the discovery of the cyclic GMP-gated conductance (Fesenko, Kolesnikov & Lyubarsky, 1985) and the identification of this conductance with the light-sensitive conductance (Fesenko *et al.* 1985; Yau & Nakatani, 1985*b*; Matthews, 1987), as well as the identification of cyclic GMP as the internal transmitter. A theory of phototransduction which proposes that cyclic GMP acts as the transmitter predicts the existence of several kinetic limitations intrinsic to the chain between isomerization and closure of the cyclic GMP-gated conductance. Two such limitations are (1) the rate of unbinding of cyclic GMP from the conductance and (2) the maximal rate of hydrolysis of cyclic GMP by light-activated phosphodiesterase. With these predicted limitations in mind, we have examined the kinetic behaviour of the flash photocurrents of isolated salamander rods, using recently developed methods of recording.

METHODS

Animals and preparation of isolated cells

Neotenous aquatic salamanders, *ca.* 25 cm in length, were obtained from Lowrance Waterdog Farms, Tulsa, Oklahoma. Animals were killed by instant decapitation, and pithing of head and spinal cord. Under infra-red illumination photoreceptor cells were loosened from the retina by gentle chopping with a fine, cleaned razor blade chip in a Sylgard-coated, plastic Petri dish containing Ringer solution. About 5 μl cell suspension was injected into a recording chamber, formed of two 0·17 mm cover-slips spaced 3 mm apart by a Lucite block with a right-angled notch exposing along its diagonal edge 7 mm of free meniscus. The chamber was seated in a slot on the mobile stage of an inverted microscope (Zeiss, IM-35), which was in turn mounted on a vibration isolation table (Model RS-46-12, Newport). A light-tight metal cage, mounted to the floor, enclosed the microscope. During an experiment the preparation was monitored with a silicon vidicon (N747(S), Hamamatsu), and routinely videotaped, although during periods of electrical recording the infra-red ($\lambda > 820$ nm) field illumination was sometimes extinguished to ensure complete dark adaptation.

Solutions

The Ringer solution used contained the following (mM): NaCl, 110; KCl, 2·5; $CaCl_2$, 1·0; $MgCl_2$, 2·0; $NaHCO_3$, 5; NaH_2PO_4, 1; HEPES, 10; EGTA, 0·05; glucose, 5. The pH was adjusted to 7·4 with NaOH. Ringer solution was saturated with 100% O_2 and kept in hermetically sealed vials. Intracellular solution contained the following (mM): potassium acetate, 100; NaCl, 5; $MgCl_2$, 2; HEPES, 10; EGTA, 0·1. The pH was adjusted to 7·35 with KOH.

Electrodes

Suction pipettes were prepared by the methods of Baylor, Lamb & Yau (1979*a*). For salamander rods, pipettes with apertures of *ca.* 11 μm were appropriate; these electrodes had resistances without the cell in place of *ca.* 0·4–0·6 MΩ, and about 2–3 MΩ with a rod in the constriction. Tight-seal pipettes were drawn from Corning 7502 Kovar sealing glass capillaries, 1·32 mm i.d., 2·18 mm o.d. (Houde Glass, Newark, NJ) (Rae & Levis, 1984). These pipettes had bubble numbers in methanol of 6·0–6·8 (Corey & Stevens, 1983), and resistances when filled with intracellular solution of 10–20 MΩ. We estimated the junction potential (at zero current) between the intracellular pipette and the Ringer solution in the recording chamber to be 2 mV; the membrane potentials we report (Table 1) can be corrected for this effect by subtracting 2 mV.

Electrical recording

Suction electrode currents were recorded with a current-to-voltage converter like that used by Baylor *et al.* (1979*a*), with bandwidth limited to 1 kHz; salt bridges were made of agar/saturated KCl. Intracellular recordings from the tight-seal electrode were made with a commercial recording system (Dagan, Model 8900, Minneapolis, MN), with a 1 GΩ feed-back resistor headstage, run at 10 KHz bandwidth. Both suction electrode and intracellular electrode signals were conditioned by 4-pole low-pass R–C cascade filters (Model 3323, Krohn-Hite, Avon, MA). The filtered suction electrode and intracellular signals, together with markers for the flash, were continuously recorded on a multi-channel FM tape-recorder (Model 3500, Thorn EMI) with a voice track. Step responses of the full recording system for different tape speeds and filter bandwidth settings for each electrode's signal were determined. During the experiment cell responses were also recorded on a strip chart (Hewlett Packard Model 7402).

Stimulus control and light calibration

A four-channel optical system was mounted external to the light-tight cage on the vibration isolation table. Two field planes conjugate with the image plane of the inverted microscope were defined just external to the light cage behind a beam-splitter. One field plane contained an aperture that was illuminated solely with infra-red light from a tungsten–halogen lamp in a light-tight housing filtered with a Wratten 87C filter; this channel served for general background illumination during the location of cells, positioning in the suction pipette, etc. The second field plane contained a rectangular aperture formed of razor blades. Three channels of the optical system illuminated the latter aperture. One, taken from a second port on the aforementioned housing, illuminated it with infra-red light. Light in a second channel illuminating the rectangular aperture came from a grating monochromator (Jobin-Yvon Model H-20, Instruments SA, Metuchen, NJ; 8 nm full bandwidth) illuminated with a second tungsten–halogen lamp with a highly stabilized d.c. power supply (Model QB12-4, Sorenson). The third channel illuminating the rectangular aperture was provided with a custom xenon flash unit with 300 J energy storage, and a short-arc flashlamp tube (Model 3P-4/FXP-864, EG & G, Salem, MA).

The channel containing the xenon arc and that containing the monochromator each had a 4-log-unit Inconel circular neutral density wedge (part No. A-6040, Kodak, Rochester, NY) mounted on a stepping motor with 180 positions. An electromagnetic shutter (Model 225, Uniblitz, Rochester, NY), used for timing monochromatic flashes, and a holder for calibrated carbon neutral filters (Kodak Wratten 96) were mounted in the common path of the two stimulus beams. The Inconel wedges were calibrated at 0·1 log unit steps at 500 nm. The wedge calibration curves were kept in tables in the computer routine that controlled the stimulus timing and intensity during the experiment.

Absolute calibration of monochromatic light fluxes at the microscope field plane were made with a Pin-10DB photodiode (United Detector Technology) operated in photovoltaic mode, calibrated

in September, 1986, by the National Research Council, Ottawa, Canada. Measurements showed that the light outside the monochromator passband seen by the photodiode was negligible (total integrated stray light, less than 2%). Calibrations of the 500 nm flux at the microscope stage were repeated over the period of these experiments, and were found to be stable within 5%. Maximal monochromatic flux density, obtained by dividing quantal flux by the area of the stimulus field stop image, was $5{\cdot}21 \times 10^5$ quanta μm^{-2} s^{-1}. The flash pulse duration was 21·8 ms, with rise and fall times *ca.* 500 μs. Thus, the total quantal energy density in an unattenuated 500 nm flash was $1{\cdot}14 \times 10^4$ quanta μm^{-2} $flash^{-1}$.

We measured the effective quantal flux parallel to the rod discs as follows. A linear polarizer (extinction ratio, 10^{-4}; part No. 03-FPG-005, Melles Griot, Irvine, CA) was positioned with its e-vector preference plane aligned perpendicular to the axis of the suction pipette over the calibrating photodiode, and quantal flux density at the image plane determined. A correction (0·18 log units) for the optical density of the polarizer not due to polarization was obtained by placing a second identical polarizer parallel to the first and noting the additional attenuation. It was thus found that 65% of the 500 nm light energy propagated through the condenser was available to excite rhodopsin molecules lying in the plane of the discs, or equivalently that the flash energy density projected in the disc plane was $7{\cdot}41 \times 10^3$ quanta μm^{-2} $flash^{-1}$. No additional correction factors were applied to the quantal energy density for the small tilt (*ca.* 15 deg) of the suction electrode relative to the image plane, or for the fact that the dichroic ratio of the rod is not infinite, or for loss of light at the air–glass interface of the chamber, or due to scattering by the suction electrode holding the rod.

The duration of the xenon flash was measured with a photodiode having a manufacturer's specified rise time of *ca.* 100 ns. An inset in Fig. 4 shows a tracing of the diode response to the flash. The flash trigger circuit had a built-in 10 μs delay. From the base, the flash rises to peak in about 5 μs; it reaches its 75th energy percentile in 22 μs, and its 90th energy percentile in 38 μs. In order to maximize the quantal flux density delivered to cells by the xenon flash, the latter was not filtered spectrally. However, its effective energy density at 500 nm was determined by routinely stimulating each cell with a few 500 nm monochromatic flashes prior to any stimulation with the xenon flash. Comparison of the waveforms of the photocurrents of cells stimulated with both flashes showed that the maximal 500 nm, 22 ms flash was equivalent to the xenon flash with 2·9 log units of interposed neutral filters. Thus, the maximal xenon flash had an equivalent energy density at 500 nm projected parallel to the rod discs of $5{\cdot}9 \times 10^6$ quanta μm^{-2} $flash^{-1}$.

The collecting area A_c of each rod (Table 1) was estimated by computing the integral

$$A_c = 2L \int_0^r \{1 - \exp[-2(\ln 10) D\sqrt{(r^2 - x^2)}]\}\, dx,$$

where r is the radius and L the length of the outer segment in μm measured from the videotape record, D the specific optical density in optical density units/μm for light linearly polarized parallel to the plane of the discs (Liebman, 1962). Since the collecting area of the rods in our sample varied from 70 to 153 μm^2 (see Table 1), for simplicity we have specified flash intensity as *fraction rhodopsin isomerized*, computed as $f_I = (A_c Q\gamma)/(V[\mathrm{Rh}])$, where Q is the flash energy density at 500 nm in the plane of the discs, γ the quantum efficiency of isomerization, V the total volume of the outer segment and $[\mathrm{Rh}] = 0{\cdot}003$ M is rhodopsin concentration referenced to the total volume. Assuming that two-thirds of the quanta absorbed by rhodopsin cause isomerization (Dartnall, 1972; Baylor, Lamb & Yau, 1979*b*), we estimate that the most intense xenon flash for the standard discharge *isomerized* 7·6% of the rhodopsin molecules in a salamander rod. In a few experiments we used a higher energy discharge which produced about 2·5 times the rhodopsin-equivalent quantal flux density of the standard flash.

Experimental procedure

With the chamber containing cells retracted, a fresh intracellular pipette was mounted in its pipette holder, and the tip was positioned in air under infra-red video control at a position predetermined in all three co-ordinates. A mechanical stop on the Huxley micromanipulator allowed the position to be locked in; the pipette was then retracted along a single axis. After this alignment, the chamber was returned to position, the suction electrode brought in, again along a single axis with a stop. A rod was then pulled into the suction electrode, and positioned about

25 μm off the floor of the chamber in a standard position in x–y co-ordinates. After control data were taken, the intracellular pipette was advanced blindly (the light-cage having been closed) in one motion to its pre-set stop, which was almost always within 25 μm of the cell, as seen on the video monitor. The final approach of the intracellular pipette was made under video control using an hydraulic advance, uncoupling the experimenter from the table. A balloon kept steady pressure on the intracellular electrode until a stopcock was turned to allow mouth suction control for tight-seal formation. This protocol usually allowed a patch attempt to be made within 30 s or so after the tight-seal pipette was advanced into the chamber, greatly diminishing the probability that the pipette tip would be soiled prior to the patch attempt.

During the period while the tight-seal pipette was being positioned apposite the cell membrane, in voltage clamp mode an offset potential was introduced to bring the amplifier d.c. current to zero, and the resistance of the pipette was measured by reading the differential current produced by a command pulse. After a tight-seal was formed to the membrane, capacitance compensation was adjusted to null the residual transient caused by the pulse, the series resistance compensation was set to the measured pipette resistance, and the command potential was switched on to the pre-set value -25 mV. The seal resistance was not routinely measured, being always in excess of 1 GΩ. A random sample of eleven rods patched between May and July, 1986, however, had a mean (± 2 S.E.M.) seal resistance of $2{\cdot}9 \pm 0{\cdot}9$ GΩ. Post-experiment transient averaging of the response to a 2 mV command voltage pulse recorded during the period after gigaseal formation and nominal capacity compensation revealed an average of less than 1 pA of uncompensated stray capacitance.

A brief mouth suction burst the membrane patch. In voltage clamp mode, the experimenter adjusted the d.c. command potential to the zero-current holding potential, and series resistance compensation was readjusted to the maximal value accepted without amplifier ringing, typically 13–40 MΩ, rarely more than twice the measured electrode resistance. In about 20% of the cells recorded from, a poor but definite intracellular access was apparent almost immediately upon patching. In these instances standard capacitance compensation values were employed, although series access compensation was performed in the same fashion as for the other 80% of the rods. During the acquisition of flash response data infra-red illumination was confined to periods between responses or to the saturated phase of responses.

Data reduction

Videotapes of each experiment were carefully reviewed to correlate electrical responses with cell morphology and position in the suction pipette. Cell and pipette outlines (e.g. Fig. 9) at the recording time nearest the moment of interest were traced from the video screen on transparent overlays. Cell dimensions were determined from these overlays.

Electrical responses from the cells were recovered from the FM tape off-line with an LSI 11/23 computer. For recovering data at greater bandwidth a transient recorder and signal averager (Model 4203, EG & G, Princeton, NJ) was employed. This allowed sampling intervals as brief as 5 μs. The EG & G recorder facilitated averaging many cycles of the whole-cell current transients from which membrane resistance and capacitance were estimated (see Table 1, below).

Terminology

Throughout this paper we use the term 'flash photocurrent' to refer to any current difference from baseline recorded by a suction electrode from an outer segment following flash illumination. Here we report evidence that supports the hypothesis that flash photocurrent can be analysed into three distinct components of membrane current: light-sensitive current proper; displacement current; 'exchange' current.

RESULTS

Electrical limitations of photoresponse kinetics

Flash responses of a rod recorded simultaneously with suction and intracellular electrodes are shown in Fig. 1, which is divided into an upper panel (labelled Voltage clamp) and a lower panel (Current clamp). In each panel are shown three traces; the upper trace in each case is the current recorded by the suction electrode; the middle

trace is the record of the intracellular electrode; the lower trace is a stimulus marker trace, showing the points at which 22 ms, 500 nm flashes were given. The sequence of events leading to gigaseal formation and whole-cell access is shown in the upper panel. The thick middle trace shows a period during which the intracellular electrode

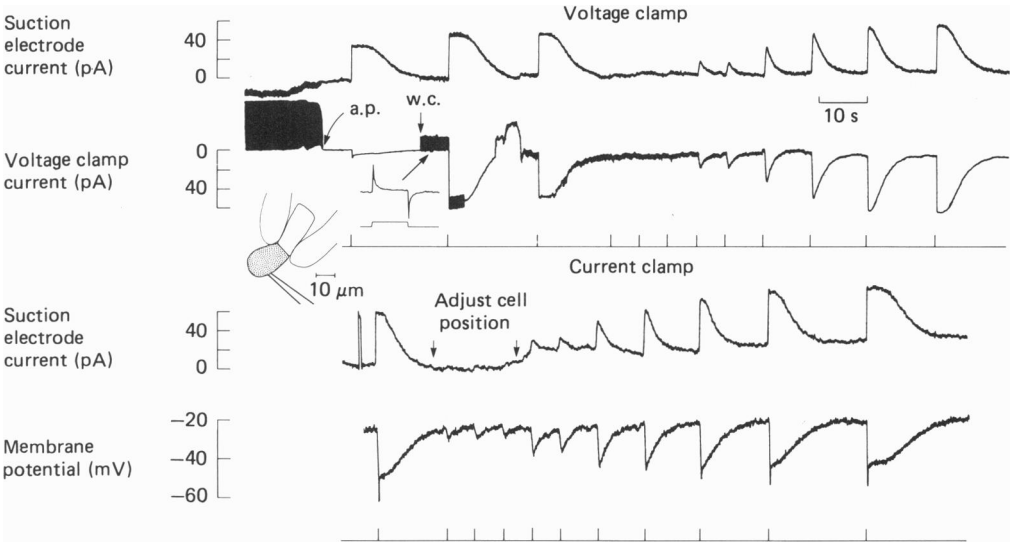

Fig. 1. Strip chart record of an experiment in which the photoresponses of a rod were measured simultaneously with a suction electrode and an intracellular tight-seal electrode, both in voltage clamp and in current clamp modes. The configuration of the cell and the electrodes is shown in an inset, which is a tracing from a videotape record of the experiment. An expanded view of the clamp response immediately after intracellular access is shown just below the trace (with an arrow pointing to the segment from which it was recovered). No series resistance compensation was applied in this experiment. The stimulus marker trace below each pair of traces indicates times where 22 ms, 500 nm flashes were given. Rod a of Table 1.

was positioned in apposition to the exposed inner segment membrane. During this period the amplifier was in voltage clamp configuration, and a 1·0 mV, clamp command pulse was applied; from the clamp response the resistance of the pipette was estimated to be 15 MΩ. At the point marked 'a.p.' an attached patch or gigaseal was formed. A light flash given right after attachment produced a small response in the clamp, indicating some intracellular access. At the point marked 'w.c.' whole-cell access was gained by a pulse of negative pressure; the holding potential was adjusted to the zero-current holding potential of −22 mV. A marked change in the clamp response to the 1 mV command pulse was observed after intracellular access was gained, owing largely to the repetitive charging of the membrane capacitance. The clamp transient response is shown on an expanded time base as an inset with an arrow pointing to the record segment from which it was recovered. Estimates of the slope resistance and membrane capacitance derived from analysis of the clamp transient were $R_m = 1120$ MΩ, $C_m = 23$ pF (see Table 1, row a). After a series of flashes of graduated intensity was delivered, the recording mode was switched from

TABLE 1. Structural, electrical and kinetic parameters of rods stimulated by intense flashes

1 Rod	2 Figures	3 A_c (μm^2)	4 A_{tot} (μm^2)	5 V_{rest} (mV)	6 R (MΩ)	7 C (pF)	8 t_{int} (ms)	9 ΔV_{max} (mV)	10 $J^{cc}_{tot,se}$ (pA)	11 τ_{cc} (ms)	12 $J^{vc}_{tot,se}$ (pA)	13 $J^{vc}_{tot,wc}$ (pA)	14 τ_{vc} (ms)	15 C_{os} (pF)	16 C'_{os} (pF)	17 C''_{os} (pF)
a	1,2,3*A*	99	2360	−25	1120	23	2·20	−37	50	20·0	45	56	—	9·9	—	—
b	9*F*	70	1890	−22	690	22	0·98	—	—	—	48	56	2·5	11·9	—	—
c	—	84	2220	−25	671	20	2·20	−38	27	24·5	25	44	3·4	11·1	—	7·0
d	—	114	2490	—	—	—	—	(−28)	45	25·0	—	—	—	13·6	—	—
e	—	104	2310	—	—	—	—	(−22)	42	12·3	—	—	—	13·7	—	—
f	4	106	2540	—	—	—	—	(−15)	40	10·0	—	—	—	17·9	—	—
g	14*D*	152	3140	—	—	—	—	(−33)	50	19·8	—	—	—	13·3	—	—
h	—	112	2600	—	—	—	—	(−27)	36	39·0	—	—	—	12·3	—	—
i	5*D*, 8*A*, 9*D*	90	2190	−21	300	26	1·46	−27	35	27·0	50	82	2·9	14·3	13·5	16·0
j	8*B*, 9*E*	83	2960	−25	1100	23	1·17	—	—	—	45	70	2·8	14·6	9·0	—
k	—	125	2760	−25	200	27	1·74	−25	25	7·7	31	48	3·0	14·5	7·0	5·0
l	—	111	2460	−23	310	30	1·36	−22	33	7·0	26	52	2·7	8·8	6·0	7·0
m	—	138	2780	—	—	—	—	(−19)	60	14·3	—	—	—	15·9	—	—
n	—	153	3050	—	—	—	—	(−20)	30	15·5	—	—	—	16·6	—	—
o	5*C*, 9*C*	128	2690	−28	490	32	1·01	−51	76	15·2	80	120	2·7	12·2	10·6	9·1
p	14*E*	146	2852	—	—	—	—	(−23)	32	9·9	—	—	—	10·1	—	—
q	14*F*	153	2970	−13	200	31	1·76	−36	36	8·5	32	78	4·5	10·3	8·0	4·0
r	5*A*, 9*A*	132	2520	−22	790	20	0·51	−35	42	10·5	48	70	2·0	11·9	6·9	10·5
s	5*B*, 9*B*	114	2460	−31	610	23	0·69	−44	42	12·7	45	65	2·5	10·6	—	11·0
t	10	70	2100	−23	650	26	0·48	—	30	—	0	45	2·5	6·1	*5·0	—

Each row a–t gives data from a different rod. The columns 1–20 are identified as follows: Column 1: rod identity. Column 2: Figures in the paper showing data from the rod. Column 3: collecting area of the rod (A_c), as defined in Methods. Column 4: total surface area of the rod (A_{tot}) estimated from the videotape record, as described in Methods. Column 5: resting membrane potential (V_{rest}) of cells penetrated by tight-seal electrodes, measured as the zero-current holding potential. Column 6: slope resistance of the rod at rest, obtained from the sustained component of the clamp response under voltage clamp to a 1–2 mV command pulse. Column 7: total capacitance of the rod, estimated by dividing the total charge in the transient component of the clamp response to a command pulse by the voltage of the pulse. Column 8: clamp integrating time t_{int}, defined as the charge under the transient component of the clamp response to a voltage pulse divided by the maximal transient current excursion; used as a conservative estimate of the clamp setting time. Column 9: maximal deviation of the photovoltage from the resting potential ($\triangle V_{max}$) in response to an intense flash. The absolute membrane potential at peak photovoltage may be computed by summing the values in columns 5 and 9. The values in parentheses represent photovoltage maxima estimated by integrating difference currents, shown in Fig. 7*B*. Column 10: maximal photocurrent recorded by the suction electrode under current clamp ($J^{cc}_{tot,se}$) or from a cell not penetrated by a tight-seal electrode. Column 11: time constant of the exponential curve fitted to the latter two-thirds of the photocurrent under non-voltage-clamp conditions (τ_{cc}) (as in Figs 4 and 5). Column 12: maximal photocurrent recorded by the suction electrode under voltage clamp $J^{vc}_{tot,se}$. Column 13: maximal photocurrent recorded by the voltage clamp electrode under voltage clamp ($J^{vc}_{tot,wc}$). Column 14: time constant of the exponential best fitting the voltage clamp photocurrent (τ_{vc}) (as in Fig. 9*A–F*). Column 15: estimate of the capacitance of the portion of the outer segment in the suction electrode C_{os}, determined by multiplying the surface area computed from the videotape record by the specific capacitance 1 μF/cm^2. Column 16: estimate of the capacitance of the portion of the outer segment in the suction electrode obtained by analysing the suction electrode's response to a command pulse applied through the voltage-clamping electrode (C'_{os}). Column 17: estimate of the capacitance of the portion of the outer segment in the suction electrode (C''_{os}) computed as described in the legend of Fig. 5.

Dashes in Table 1 signify either that the measurement did not apply (e.g. some cells were recorded from with suction electrode only) or that some limitation prevented accurate determination (e.g. suction electrode bandwidth was inadequate in some experiments to permit recovery of the response to a clamp command voltage pulse).

* Note that for the rod of row t, the inner segment was in the suction electrode.

voltage clamp to current clamp; this switch occurred immediately at the end of the upper trace, and is signalled by the spike shown in the suction electrode trace in the lower panel. The middle trace in the lower panel thus represents the photovoltages produced in current clamp mode. The entire cycle (voltage clamp light intensity series, current clamp series) was repeated another time before terminating the experiment.

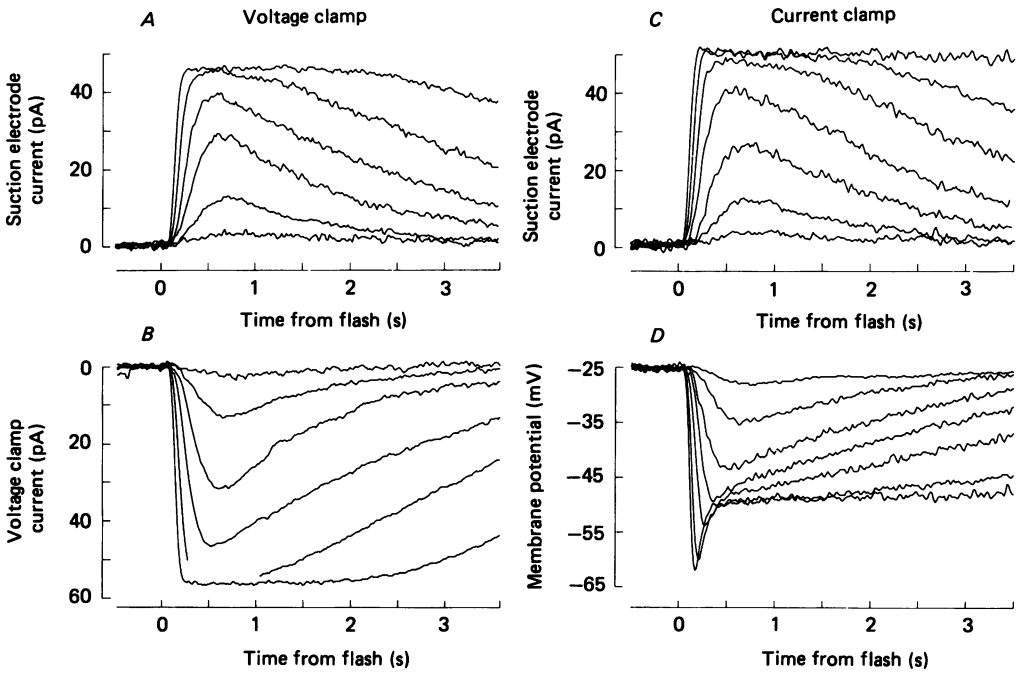

Fig. 2. Flash responses of the cell of Fig. 1 collected and shown on an expanded time base. In the left half of the Figure simultaneously recorded suction electrode (*A*) and voltage clamp responses (*B*) are shown; in the right half, simultaneously recorded suction electrode (*C*) and current clamp (*D*) responses. The flashes were graded in 0·5 log unit steps, with the dimmest flash estimated to produce *ca.* 5 isomerizations, and the most intense, 6000 isomerizations ($10^{-6\cdot1}$ fractional rhodopsin isomerization). Note that the most intense flash given under current clamp, was not given under voltage clamp. For the dimmer flashes, several responses were averaged. The interrupted trace in *B* occurred due to an overflow in the FM recorder, which was corrected before the most intense flash was delivered under voltage clamp. This interruption was not present in the original strip chart record, which was used to produce Fig. 1.

The simultaneously, intra- and extracellularly recorded photoresponses of the cell of Fig. 1 are collected and presented on an expanded time base in Fig. 2. The left half of the Figure shows the responses obtained under voltage clamp. Both suction electrode and voltage clamp electrode records here (and throughout the paper) are presented in 'amplifier sign convention', i.e. an upward trace represents a positive current flowing into the current-to-voltage converter circuit. Under voltage clamp, the suction electrode and voltage clamp electrode record oppositely signed photocurrents of the same waveform because they are electrically connected to opposite sides of the membrane, and because, during a light response the voltage

clamp electrode must supply the current whose flow through the outer segment membrane light has blocked. The whole-cell voltage clamp recovered a somewhat larger maximal photocurrent than the suction electrode (56 *vs.* 45 pA for the last flash in the upper panel) because the suction electrode is an imperfect collector of outer segment membrane current, owing to the relatively low seal resistance (*ca.* 2·5 MΩ) of the rod in the suction pipette and its lengthened region of contact with the cell.

The right half of Fig. 2 collects the extra- and intracellularly recorded photoresponses obtained under current clamp. A distinctive feature recorded by the intracellular electrode in this mode is the transient peak or 'nose' characteristic of amphibian rod photovoltages. In contrast to the effect of recording mode on the waveform of the intracellularly recorded photoresponses, little if any effect of mode is seen in the waveforms of the outer segment photocurrents recorded by the suction electrode. In particular, the nose, which is so prominent in the photovoltages, is not seen in the outer segment photocurrents recorded simultaneously by the suction electrode. Indeed, as previously reported by Baylor & Nunn (1986), the responses recorded by the suction electrode under voltage clamp have waveforms nearly identical to those it recorded under current clamp. Two unique properties of the rod membrane are thought to be responsible for this congruence of outer segment photocurrents under current and voltage clamp. The first property is the very shallow I–V relation of the light-sensitive current in the range of membrane potentials over which the photovoltage operates (Bader, MacLeish & Schwartz, 1979; Baylor & Nunn, 1986). The second property is the virtual absence from the outer segment membrane of appreciable conductance other than that which carries the light-sensitive current (Baylor & Lamb, 1982; Baylor & Nunn, 1986). An important consequence of these properties is that the light-sensitive current acts as a *current source* whose modulation reflects the underlying process controlled by light, and not the membrane potential. On the time-scale of these responses, the photovoltage of the cell can be modelled as the voltage response of an RLC circuit whose resistive and inductive components are determined by the inner segment membrane and whose input is the outer segment light-sensitive current (Baylor, Matthews & Nunn, 1984).

A notable congruence of the rod photoresponses of Fig. 2 can be observed in a comparison of the extracellularly recorded photocurrents and intracellularly recorded photovoltages measured simultaneously under current clamp. This comparison is made explicit in Fig. 3*A*, in which the photovoltages of the lower half of Fig. 2 have been inverted, and scaled by a common factor. Over the entire range of intensities the photovoltages and photocurrents can be brought into congruence in the early part of their rising phase by a single scale factor. As reported by Baylor *et al.* (1984), at the lowest flash intensity the photovoltage and photocurrent have similar, but not identical waveforms. At higher flash intensities the photovoltage diverges from the simultaneously recorded photocurrent at ever earlier times. Fig. 3*B* presents data from another cell showing the same correspondence; the phenomenon was confirmed in a third (data not shown). The congruence of Fig. 3 would be expected if the slope resistance of the rod remains little altered during the period of correspondence. In reasonable agreement with this explanation is the fact

that the scale factor for congruence for the rod of Fig. 3*A* is 0·8 mV/pA or 800 MΩ (assuming the suction electrode collected 80% of the photocurrent), as compared to the slope resistance of 1120 MΩ estimated from the analysis of the d.c. component of clamp response to the 1 mV command pulse.

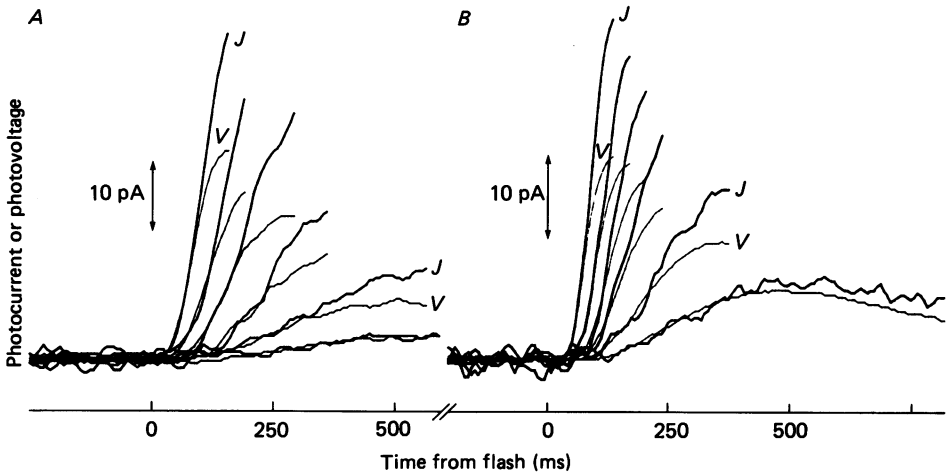

Fig. 3. Comparison of photocurrents recorded from outer segments of two rods with simultaneously recorded photovoltages. Photocurrents (*J*) and photovoltages (*V*) were independently recovered from the FM tape record. After inversion, the complete family of photovoltages was scaled by a common factor, which brought the two types of photoresponses into correspondence over a segment of time from the flash. *A*, data from Fig. 2 replotted. *B*, data as in *A* from another rod. Resting potential was −23 mV; maximal hyperpolarization −44 mV from rest. The scale factor for correspondence was 1·8 mV/pA. Since only 64% of the rod outer segment was past the point of the maximal constriction in the suction pipette, an estimate of the instantaneous resistive load of the photovoltage is 1·15 mV/pA = 1150 MΩ. Slope resistance at rest estimated from response to a 1 mV clamp command pulse under voltage clamp was 1000 MΩ.

The correspondence in Fig. 3 between photovoltage and photocurrent at early times after a flash can be expected if the light-sensitive conductance makes negligible contribution to the slope conductance of the rod at rest and if any voltage-dependent conductances are activated or deactivated slowly in comparison with the light-sensitive conductance. None the less, as noted by Baylor *et al.* (1984), flashes of intensity sufficient to produce rapid hyperpolarization should produce a divergence between photovoltage and photocurrent, even at early times. This divergence is predicted because a capacitative current, C_{os} (dV/dt), necessarily contributes to the photocurrent recorded by the suction electrode (here C_{os} represents the capacitance of the outer segment in the suction electrode). In the data of Fig. 3*A* the maximum value of dV/dt was 0·38 V/s; assuming a specific capacitance of 1 μF/cm^2, we estimated C_{os} = 9·9 pF from the videotape record (Table 1, row a, column 15), so given 80% suction electrode collecting efficiency, one predicts a maximal capacitative current of 3·0 pA. For the rod of Fig. 3*B* the maximal capacitative current predicted is about 4 pA. Because the photovoltage is a hyperpolarizing response, the predicted displacement current is outer-segment-inward. Thus one

would expect the photocurrent recorded by the suction electrode from the outer segment under voltage clamp to the most intense flashes used in the experiments of Figs 1–3 (producing about 10^5 isomerizations) to rise above that measured under current clamp by about 3–4 pA. This is at the edge of reliable detection under the limited number of flash repetitions used in the experiments just described. We shall show, however, that for more intense flashes a component of photocurrent attributable to capacitative charging is readily measurable.

All four families of responses in Fig. 2 share the common property that the maximum velocity continues to increase monotonically with increasing flash intensity over the range of intensities used in the experiment, as expected from the work of Penn & Hagins (1972) and Baylor *et al.* (1974). A primary goal of this investigation was to determine whether or not this monotonicity continues over a much greater flash intensity range. Figure 4 shows the result of an experiment in which suction electrode responses were recorded from a rod stimulated with 20 μs Xenon flashes up to 10^4 times more intense than the most intense flash used in the experiment of Figs 1 and 2. These data show that flashes that isomerized more than 0·01 % of the rod's rhodopsin produced photocurrents whose rising phase (as opposed to latency or delay time) had a nearly invariant form, when translated on the time axis. This invariance is better revealed in the lower panel, in which the photocurrents to the second and third most intense flashes of the upper panel have been displaced on the time axis for maximal coincidence with the photocurrent produced by the most intense flash. An apparently similar translation invariance was found by Penn & Hagins (1972, Fig. 11) in their study of rat rod photocurrents for flashes producing more than 7×10^5 isomerizations per rod (*ca.* 0·7 % bleach). In the results shown in Fig. 4, not only do the laterally translated photocurrents coincide over more than 50 % of their range, but also they are reasonably well described as a simple exponential curve, with a time constant of 10 ms.

Translation invariance of photocurrents of rods stimulated with 20 μs flashes isomerizing greater than 0·01 % of the rhodopsin and recorded only with a suction electrode was confirmed in three other cells, using the same protocol as in the experiment of Fig. 4. For the four cells studied with that protocol the best fitting exponentials had time constants of 10·0, 12·3, 19·8 and 36 ms, respectively (Table 1, rows f, e, g and d). The total surface areas of these four cells estimated from our video records were 2490, 2313, > 2540 and 3138 μm^2, with the third cell's surface being a lower bound because its tip was off the video screen. If the specific capacitance of the rod membrane is 1 $\mu F/cm^2$, the expected capacitances of these rods would be 24·9, 23·3, > 25·4 and 31·4 pF, respectively. Furthermore, if the effective resistance of the membrane during the photocurrent were about 1 GΩ, then one would expect cell time constants of 25, 23·3, > 25 and 31 ms respectively, in rough correspondence with the observed photocurrent decay time constants. Closer correspondence might come about if the resistance were as low as 0·5 GΩ, a value within the range 0·2–1·1 GΩ found for direct measurements in twelve rods (Table 1, column 6). These observations suggested to us the possibility that the limiting time course of the photocurrent seen in Fig. 4 might be the result of passive electrical properties of the rod membrane, and not of the transduction mechanism *per se*. The photocurrents of these rods could be composed of a fast (net) outer-segment-outward component

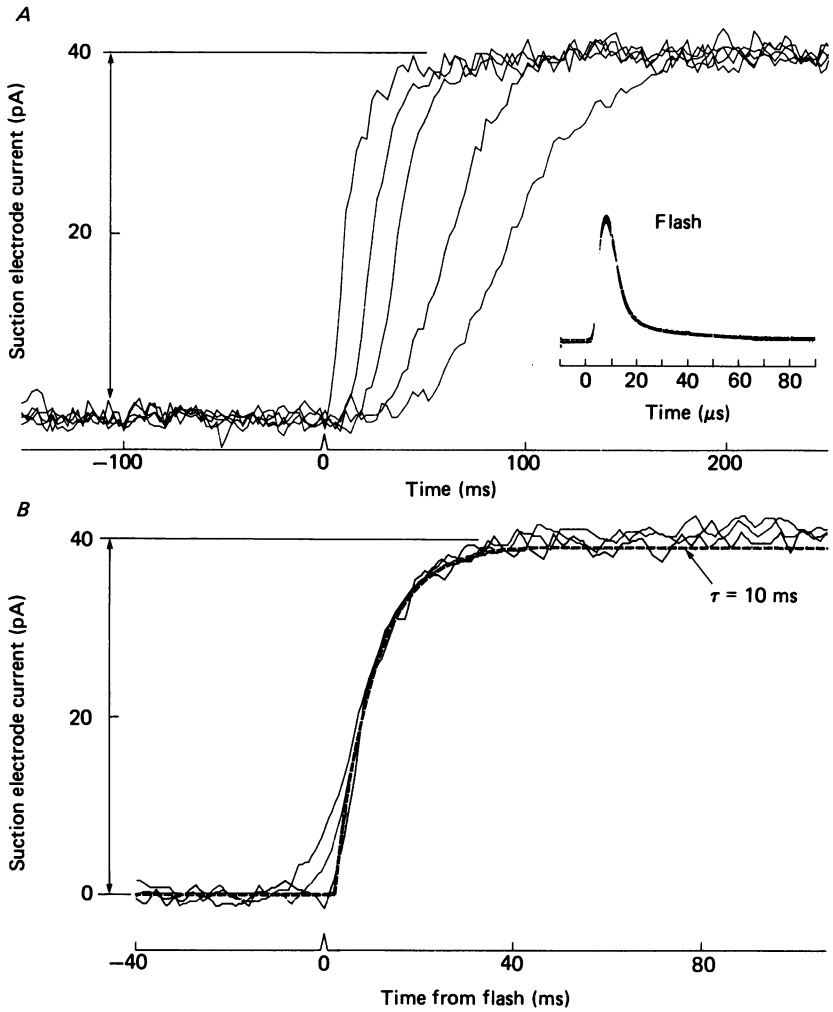

Fig. 4. Photocurrent of an isolated rod recorded with the suction electrode only, and stimulated with 20 μs xenon flashes of graded intensity. *A*, the responses are presented in absolute position. From right to left (least intense to most intense flash), the fraction of rhodopsin isomerized and number of responses averaged was $10^{-5\cdot42}$, $n = 3$; $10^{-4\cdot92}$, $n = 3$; $10^{-3\cdot92}$, $n = 2$; $10^{-2\cdot92}$, $n = 3$; $10^{-1\cdot12}$, $n = 1$. The recording bandwidth was 300 Hz; system step response had dominant exponential time constant of 1·6 ms. *B*, the responses shown in the upper panel to the three most intense flashes are shown on an expanded time base and the two to the less intense flashes ($10^{-3\cdot92}$ and $10^{-2\cdot92}$ fractional isomerization) were translated 10·4 and 21 ms respectively for optimal coincidence. An exponential (dashed line) was fitted by least squares to the combined traces; its time constant is 10·0 ms. Data from rod f of Table 1. Inset to right in upper panel shows oscillographic trace of a photodiode response to the xenon flash; note that the time base for the flash trace has units of microseconds.

driven by light, from which a transient displacement current determined by the cell time constant is subtracted.

Evidence consistent with the hypothesis that the photocurrent rate limitation seen in Fig. 4 owes to a capacitative or displacement current, and that the closure of the

light-sensitive conductance in response to intense flashes is several times faster than the time course of suction electrode current measured in non-voltage-clamped cells is presented in Fig. 5. The Figure presents simultaneously recorded intracellular and suction electrode photoresponses from four cells in four panels, *A–D*. Each panel consists of an upper and a lower section. In the upper section are presented three data traces: the two fastest rising traces (*a* and *b*) are simultaneously recorded photocurrents measured with the suction electrode and the whole-cell electrode respectively; the whole-cell voltage clamp response has been inverted to show its temporal correspondence with the suction electrode response; both responses have been normalized. Also shown in the upper panel as the slower data trace (*c*) is a photocurrent measured by the suction electrode during current clamp; the simultaneously recorded photovoltage (*e*) is shown in the lower section of each panel. In addition, two other curves are shown in each of the four panels: in the upper section of each panel the dashed trace (*d*) shows an exponential curve fit to the photocurrent (*c*) recorded by the suction electrode in the current clamp condition. In the lower panel is shown a curve (trace *f*) derived by integrating the difference in the voltage clamp and current clamp photocurrents, as described in the next paragraph.

To explain how these data can be used to deduce the displacement current that must be present in non-voltage-clamped rods, we consider the following expression:

$$J_{\text{tot}}(t) = J_{h\nu}(t) + J_{\text{ionic}}(t) + C_{\text{os}}(\mathrm{d}V/\mathrm{d}t). \tag{1}$$

Here J_{tot} is the total outer segment photocurrent recorded by the suction electrode, $J_{h\nu}$ is the light-sensitive current proper, J_{ionic} is the sum of all other ionic currents, C_{os} is the capacitance of the outer segment membrane in the suction electrode, and V the membrane potential of the rod. Suppose further that for some period of time after an intense brief flash we may write

$$J_{h\nu}(t) = g(I,t)J_{h\nu,\max}, \tag{2}$$

$$J_{\text{ionic}}(t) = J_{\text{ionic}}. \tag{3}$$

Equation (2) states that the light-sensitive current can be written as the product of a gating function, $g(I,t)$, which is dependent only on I, the number of isomerizations and on time, and $J_{h\nu,\max}$, the maximum of the light-sensitive current. Equation (3) states that all outer segment ionic currents other than the light-sensitive current proper are not functions of time on the interval of interest. It then follows by substitution and subtraction that

$$J^{\text{vc}}_{\text{tot}}(t) - J^{\text{cc}}_{\text{tot}}(t) = -C_{\text{os}}(\mathrm{d}V/\mathrm{d}t), \tag{4}$$

where the superscripts refer to the recording mode. Define $\Delta J(t)$ to be the left-hand side of eqn (4); then dividing both sides of eqn (4) by C_{os} and integrating, one obtains the prediction

$$[V(t) - V(0)] = -(1/C_{\text{os}}) \int_0^t \Delta J(t')\,\mathrm{d}t'. \tag{5}$$

The lower section of each panel *A–D* of Fig. 5 shows the results of performing this integration for each of the four rods; the predicted photovoltage (trace *f*) is shown along with that directly measured under current clamp (trace *e*). Two measures were

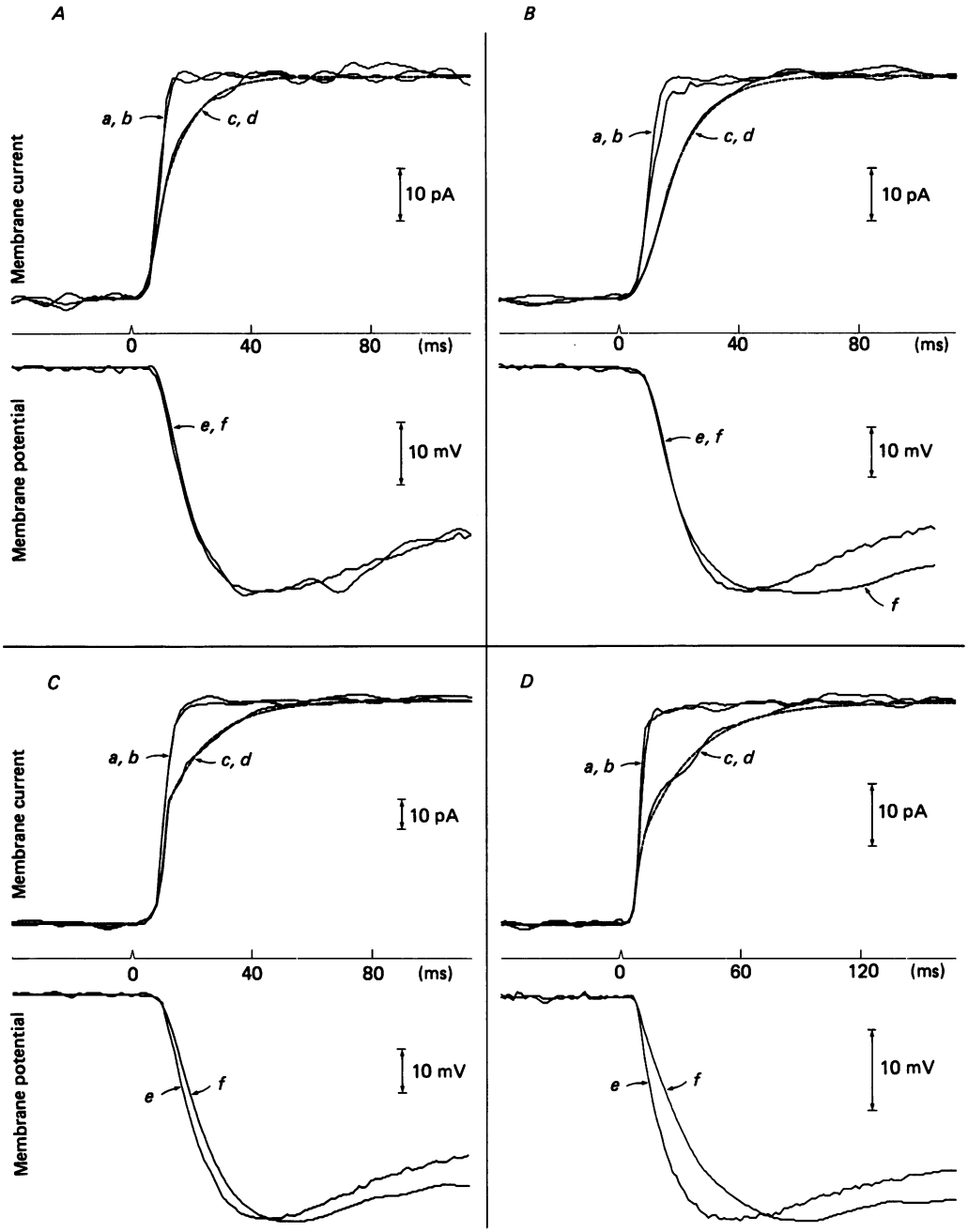

Fig. 5. Each of the panels *A–D* is a repetition of the same experiment on a different rod (rods s, r, o and i respectively in Table 1). After a cell was penetrated with a gigaseal electrode, it was stimulated under current clamp with a flash isomerizing at least 0·76% of the rhodopsin. The suction electrode current measured in response to this flash is shown as the curve labelled *c*; the simultaneously recorded photovoltage, *e*. The dashed line *d* is an exponential curve fitted by least squares to the upper two-thirds of trace *c*. The cell was allowed to recover *ca.* 2 min from the first flash, the recording mode was switched to

taken in the effort to match observed and predicted photovoltages. First, the difference current computed was in fact

$$\Delta J(t) = [(1 \pm e) J^{vc}_{tot}(t) - J^{cc}_{tot}(t)],$$

where e is an amplitude correction used to normalize the maximum of the voltage clamp response (Table 1, column 12) to that of the current clamp response (Table 1, column 10); without such normalization the integral in eqn (5) diverges. Use of the correction is tantamount to the assumption that the voltage clamp response to the intense flash obtained at one time gives the correct waveform, if not the correct amplitude, of the voltage clamp response that would have been observed at the other time when the current clamp response was obtained. The second measure taken in optimizing the fit was to treat C_{os} in eqn (5) as a free parameter, while forcing ΔV_{max} to have the value (Table 1, column 9) directly measured. This allowed comparison of the capacitance estimated with this procedure with the values estimated from measurement of the outer segment membrane in the suction pipette. The complete experiment was performed on eight rods; the estimated values of C_{os} (capacitance of outer segment membrane in suction pipette) are shown in column 17 of Table 1. A direct comparison of the difference current $\Delta J(t)$ with the derivative of the measured photovoltage (see eqn (4)) is presented in the left half of Fig. 6 for the same eight rods. Here the difference currents are presented in absolute units and the voltage derivative has been scaled for fit by eye. In the right half of Fig. 6 are presented difference currents obtained from eight rods whose photocurrents were recorded with suction electrode only. The voltage clamp response used in the computation was the average of the voltage clamp photocurrent of eleven voltage-clamped rods stimulated with flashes isomerizing 2·4% or more of the rhodopsin; the average was computed by first sliding the responses laterally for optimum coincidence. The mean voltage clamp photocurrent was positioned relative to the measured non-clamped photocurrent so that the two curves coincided at their feet. (Additional justification for using the average voltage clamp response will be given below.) Examination of the two sets of difference currents in Fig. 7 shows that the two populations do not differ systematically in either amplitude or time course. We estimated the photovoltages of the non-clamped rods of the right half of Fig. 6 by integrating the difference currents, as shown in Fig 7.

In the upper panel are presented the directly measured photovoltages of the eight rods whose data are shown in the left half of Fig. 6. In the lower panel are shown the photovoltages estimated from integrating the difference currents of the non-clamped rods whose data are shown in the right half of Fig. 6. In the latter case, the value of C_{os} used was that estimated from the membrane surface area measured in the suction pipette, assuming a specific membrane capacitance of 1 μF/cm^2. The numerical

voltage clamp, and the cell stimulated under voltage clamp with a flash isomerizing at least 0·76% of the rhodopsin. The photocurrents recorded by the suction electrode and whole-cell electrode under voltage clamp are identified as *a*, *b* in each panel; the traces have been normalized, and filtered outside the flash transition region with a Gaussian filter having a standard deviation of 3·4 ms. The curve labelled *f* was computed according to eqn (5), as described in the text. The value of *e* for the four calculations (compare columns 10 and 12 of Table 1) was −0·13, −0·06, −0·05 and −0·30.

estimates of the maximal photovoltages are shown in Table 1, column 9, in parentheses. The photovoltages estimated from difference currents resemble those obtained from direct measurements, though the two sets of photovoltages clearly do not come from the same distribution. First, the intracellularly measured hyper-

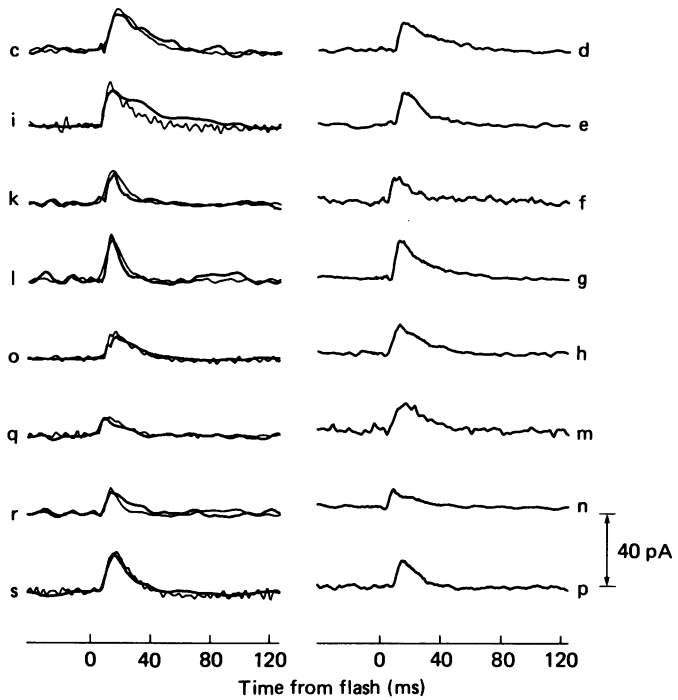

Fig. 6. Difference currents obtained by subtracting the non-voltage-clamped intense flash suction current from the voltage-clamped suction current for sixteen rods are shown as the heavy lines. The rods whose data are shown in the left-hand panel (rods c, i, k, l, o, q, r and s of Table 1) were given intense flashes under both current and voltage clamp, and their difference currents were computed directly from the two photocurrents. Also shown in the left-hand panel is the displacement current predicted by differentiating the observed photovoltage numerically, and scaling for optimum fit. The scaling parameter is an estimate of the capacitance of the outer segment in the suction electrode. The photocurrents of the rods whose data are shown in the right-hand panel (rods d, e, f, g, h, m and p of Table 1) were recorded with suction electrode only; the voltage clamp photocurrent used for the subtraction was formed by the average of eleven cells, as described in the text. The difference currents can be used to estimate the light-induced hyperpolarizations, as shown in Fig. 5. For the rods of the right-hand side of Fig. 6 the hyperpolarization was estimated by integrating the difference current, and scaling by the reciprocal of the capacitance of the outer segment estimated from measuring the outer segment membrane area and assuming a specific capacitance of 1 μF/cm^2. These estimates are shown in column 9 of Table 1 in parentheses.

polarizations peak a bit sooner than those estimated with eqn (5). This defect may in part be corrected by judicious choice of the parameter e in eqn (6), but such manipulation seems unwarranted. The second defect is that the distribution of photovoltage maximum amplitudes estimated by the difference current integration falls short of that directly measured: the mean (± 2 S.E.M.) of the eight direct

measurements was -35 ± 7 mV; the mean of the eight estimates from free rods was -23 ± 4 mV. Despite these quantitative discrepancies of the simple model of eqns (1)–(3) with data, we conclude that the evidence supports the conclusion that the photocurrent response of current-clamped or free rods to intense flashes has a rising phase whose time course is dominated by an outer segment-inward capacity current.

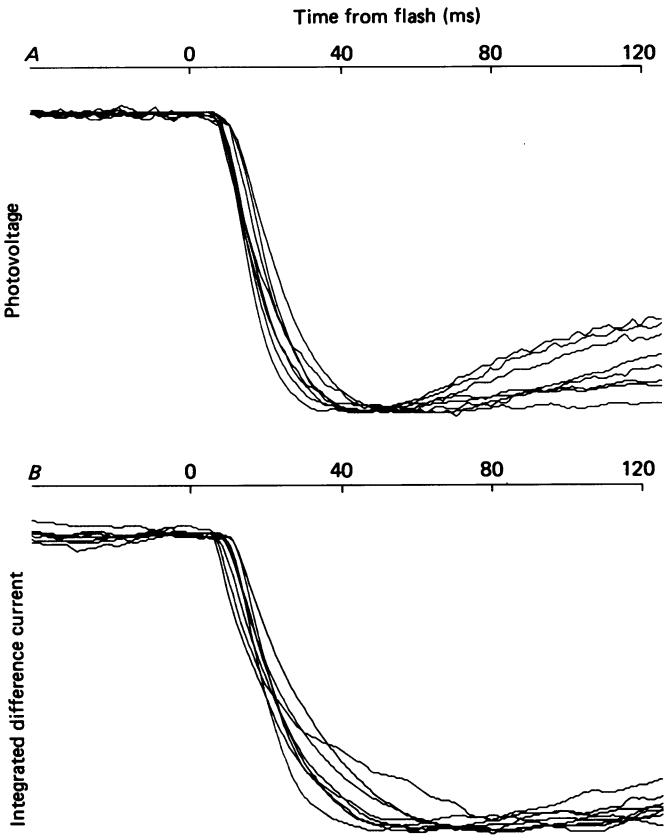

Fig. 7. Upper panel shows the directly measured intense-flash photovoltages of the eight rods whose data are shown in the left-hand panel of Fig. 6. Lower panel shows the integrals of the difference currents shown in the right-hand panel of Fig. 6. The traces in both the upper and lower panel have been normalized; the numerical value of the maxima of the traces can be found in Table 1, column 9.

Photocurrent kinetic limitations under voltage clamp

If the results presented in Figs 4–7 make a case that passive electrical properties of the rod membrane account for the photocurrent rising phase limitation observed in non-voltage-clamped rods, they leave open the issue of what limits the rising phase of the photocurrent under voltage clamp. Keeping in mind that we observed no reliable differences between the form of the photocurrent measured by the suction electrode and that measured with the voltage clamp electrode in the first 50 ms after

an intense flash with comparable recording bandwidth (see Fig. 5, traces *a* and *b* in each panel), in addressing the kinetic limitations of the voltage clamp photocurrent, we chose to concentrate our attention on the whole-cell photocurrent. The primary reason for this choice was that the suction electrode responses were inherently much

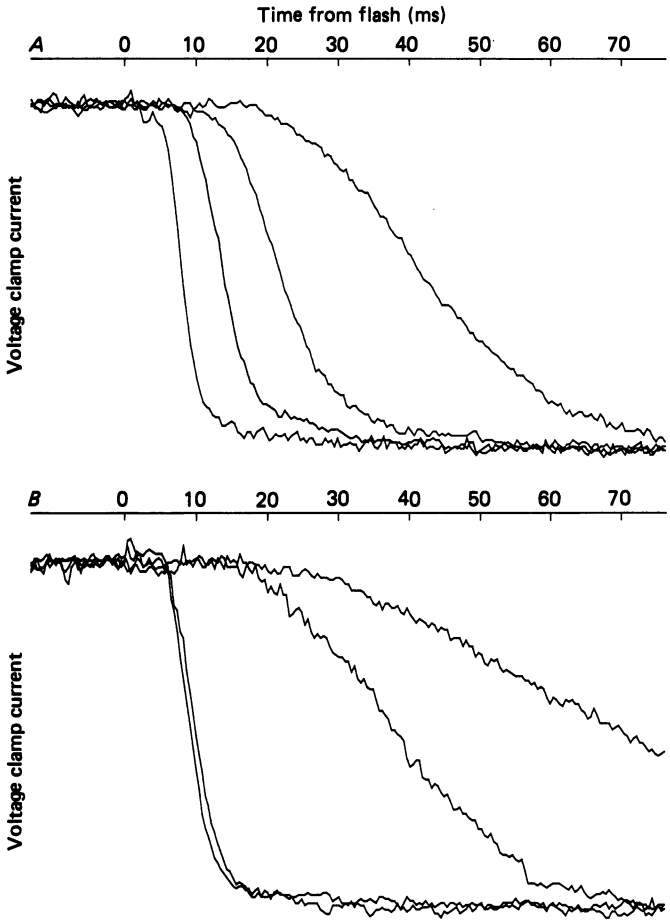

Fig. 8. Voltage clamp photocurrent recording by the clamping electrode from two different rods (*A* and *B*) in response to intense 20 μs flashes showing translation invariance of responses. *A*, rod stimulated by 20 μs flashes producing (from least to most intense) $10^{-4.92}$, $10^{-3.92}$, $10^{-2.92}$ and $10^{-1.12}$ fractional isomerization of the rod's rhodopsin. Maximal photocurrent, 82 pA; clamp integration time, 1·5 ms. *B*, rod stimulated by flashes producing $10^{-5.52}$, $10^{-4.52}$, $10^{-1.72}$ and $10^{-0.72}$ fractional isomerization. Maximal photocurrent, 70 pA; clamp integration time, 1·2 ms.

noisier at broad bandwidth than the whole-cell responses, owing to a *ca.* 1000-fold lower seal resistance. Figure 8 shows data from two voltage-clamped rods showing that a photocurrent rising phase invariance like that observed under current clamp is also seen under voltage clamp conditions. In the experiment of the Fig. 8*A* the rod was stimulated successively with saturating flashes isomerizing $10^{-4.92}$, $10^{-3.92}$, $10^{-2.92}$ and $10^{-1.12}$ (7·6%) of the rhodopsin. The rising phases of the photocurrents to the

two most intense flashes, separated by almost 2 log units, have almost the same maximal velocity. In the experiment of Fig. 8*B* the charging voltage of the flashlamp was increased 4-fold (from 0·2 to 0·8 kV). From comparison of the cell's response to just-saturating monochromatic and xenon flashes, we estimated that the flash then produced 2·5 times the rod-equivalent quanta produced by the most intense flash used in the experiment of Fig. 8*A*. We thus estimate that the two most intense flashes in the experiment of Fig. 8*B* isomerized 1·9 and 19% of the rhodopsin, respectively. Clearly, this change in fractional isomerization causes little change in the photocurrent rising phase.

To derive a clear picture of the rate-saturated photocurrent observed under voltage clamp, we measured the response of a population of rods to 20 μs flashes isomerizing 2·4% or more of the rhodopsin. Figure 9 presents voltage clamp photocurrents from six of these rods. The noisy trace in each of the six panels *A–E* is the observed photocurrent. To the left of the trace is shown a line tracing from the videotape record of the experiment. The dashed curve is an exponential curve fitted with a least-squares criterion to the photocurrent. To the right of these traces is shown the recorded response of the clamp to a 2 mV test pulse, determined shortly before the flash was delivered to the rod. Maximal photocurrents, resting membrane potentials, and clamp settling times are presented in Table 1. The latter two-thirds of the photocurrent is reasonably well described as an exponential decay, although a small systematic deviation near the saturating level was observed in each case. The mean 'photocurrent time constant' (± 2 S.E.M.) for eleven rods determined in the same fashion was $2{\cdot}8 \pm 1{\cdot}2$ ms.

It seems reasonable to believe that this 2·8 ms time constant is determined by the phototransduction gating mechanism, but *a priori* it is possible that the gating mechanism is much faster, and that a displacement current due to a voltage error between clamp and membrane might be the cause of the rate limitation. One argument against the notion that a displacement current is responsible for the voltage clamp photocurrent velocity limitation can be based upon the data in Fig. 10.

In the experiment of Fig. 10 the rod was turned around in the suction pipette, so that only the inner segment membrane (which contains voltage-sensitive, but no light-sensitive conductance) was in the suction pipette. In the left half of the Figure is shown a suction electrode response (Control) obtained during the period when the tight-seal pipette was attached to the outer segment membrane: prior to intracellular access, when the membrane potential is free to hyperpolarize, the inner segment membrane exhibits an ionic current change upon flash illumination. After intracellular access, a similar (but 50% larger) photocurrent to the control flash was observed in the voltage clamp; the suction electrode, however, showed no obvious response, indicating that the inner segment membrane did not undergo any large voltage excursion. In the right panel are shown the simultaneously recorded suction electrode and voltage clamp currents measured in response to a subsequent flash that isomerized 7·6% of the rhodopsin: again, the suction electrode recorded no obvious change in inner segment membrane current, whereas the voltage-clamp recorded a photocurrent whose latter phase is best fitted with an exponential having a time constant of 2·5 ms. It is clear that no large ionic current crossed the inner segment

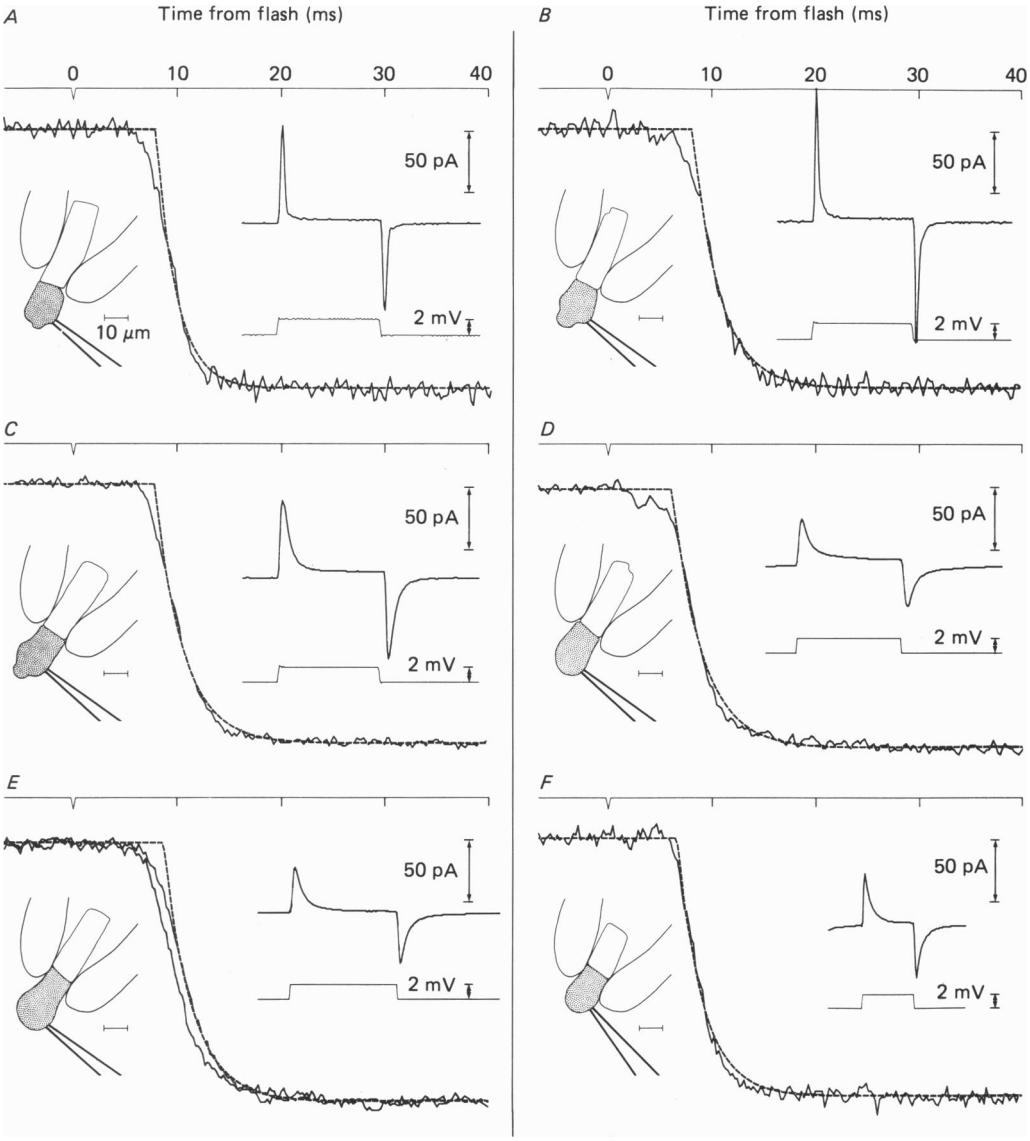

Fig. 9. Photocurrents (noisy traces) recorded by voltage clamp electrode in six rods stimulated with 20 μs flashes isomerizing 7·6% of the rhodopsin. (The rod in panel *E* was stimulated with flashes isomerizing 1·9 and 19% of the rhodopsin respectively.) The dashed line through the photocurrent is an exponential curve fitted by least squares to the latter two-thirds of the photocurrent. The inset to the left in each panel *A–F* shows a line tracing of a videotape record of the experiment, showing position of cell and recording electrodes. To the right of the photocurrent trace in each panel is shown the clamp response to a 2 mV command pulse obtained a few seconds before the flash; these responses to the command pulse represent the average of about 100 cycles; the same vertical scale applies for all the command pulse responses, but the photovoltages have been normalized. We defined the *latency* of these voltage clamp photocurrents as the intersection of the exponentials with the time axis. The identity of the rods in Table 1, maximal photocurrents, and latencies are as follows: *A*, rod r, 70 pA, 7·6 ms; *B*, rod s, 65 pA,

membrane in response to the intense flash, and thus that the membrane underwent no large voltage change. Additional quantitative analysis is required to exclude the possibility that an error voltage and attendant displacement current too fast or small to be seen in the suction electrode limited the photocurrent decay rate, however. To

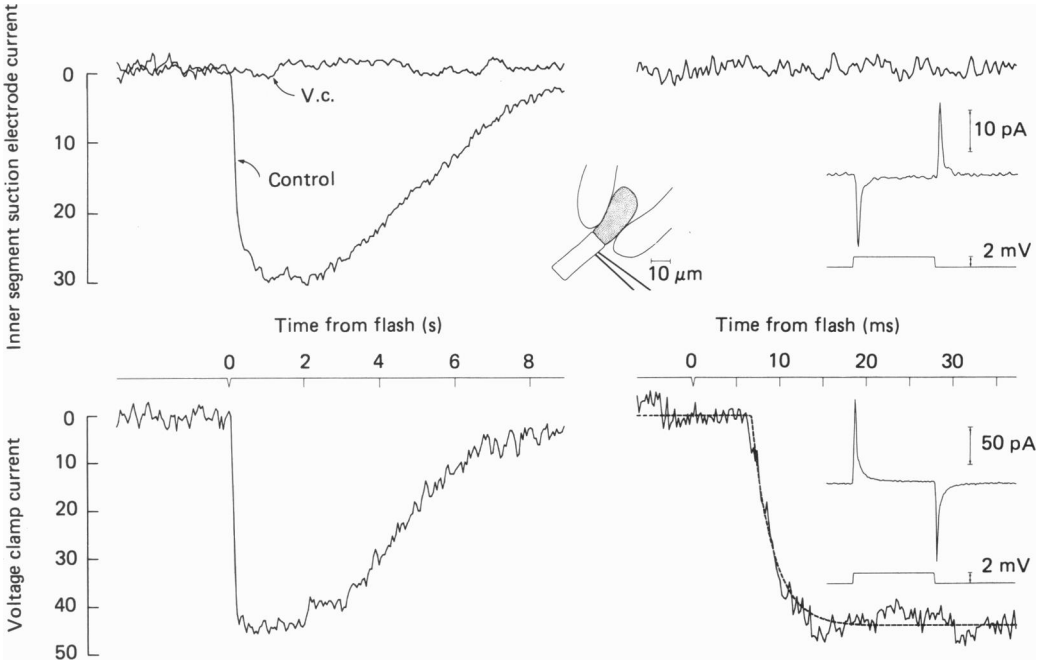

Fig. 10. Photocurrents of a rod (Table 1, row t) stimulated with an intense flash in 'outer-segment-out' configuration, as shown in the inset tracing from the videotape record of the experiment. Left-hand panel shows a control suction electrode response to a just-saturating flash obtained after an attached patch was formed to the outer segment membrane, but prior to intracellular access. After access, the voltage-clamping electrode recorded the response shown in the lower left-hand panel, while the suction electrode recorded no reliable response (trace labelled V.c.). In the right-hand panel are shown the traces recorded when the rod was stimulated with a flash isomerizing 7·6% of the rhodopsin. Also shown as insets are the responses of the clamp electrode and the suction electrode to a 2 mV command pulse, obtained by averaging about 50 cycles delivered immediately before the intense flash. Dashed curve (lower right), exponential with time constant of 2·5 ms. Nominal recording bandwidth (f_c of 4-pole filter) was 3000 Hz for the voltage clamp and 1000 Hz for the suction electrode.

effect such analysis we recovered the suction electrode response to a voltage clamp command pulse: the 2 mV clamp command produced a nearly 15 pA (largely capacitative) transient in the suction electrode. It follows that if an error voltage of even 1 mV had been present during the photocurrent response to the intense flash, it would have produced a current transient measurable by the suction electrode.

7·8 ms; *C*, rod o, 120 pA, 7·6 ms; *D*, rod i, 82 pA, 6·1 ms; *E*, rod j, 70 pA, 8·5 ms and 65 pA and 7·4 ms, respectively; *F*, rod b, 56 pA, 6·7 ms. The nominal recording bandwidth (f_c of the 4-pole filter) was 3000 Hz for cells in *A* and *B*, and 1000 Hz for the other four experiments; under these conditions the system step response had a limiting exponential rise of 160 μs in *A* and *B* and 500 μs in *C–F*.

Furthermore, if the light-triggered gating function were really a step function occurring with an absolute dead time, then the error voltage excursion can be calculated by integrating the exponential curve fitted to the photocurrent: the predicted displacement charge is $2{\cdot}5 \times 10^{-3}$ s $\times 45 \times 10^{-12}$ A $= 113 \times 10^{-15}$ C. Since the measured capacitance of the rod was 26 pF, the predicted error voltage is $(113 \times 10^{-15})/(26 \times 10^{-12}) = 0{\cdot}0043$ V, or 4·3 mV. Certainly, the greater than 10 pA inner segment displacement current that would have been caused by an error voltage of this magnitude would have been detected. Our conclusion is that the rod was effectively isopotential throughout its flash response, and that its membrane potential did not undergo a transient excursion of even a few millivolts.

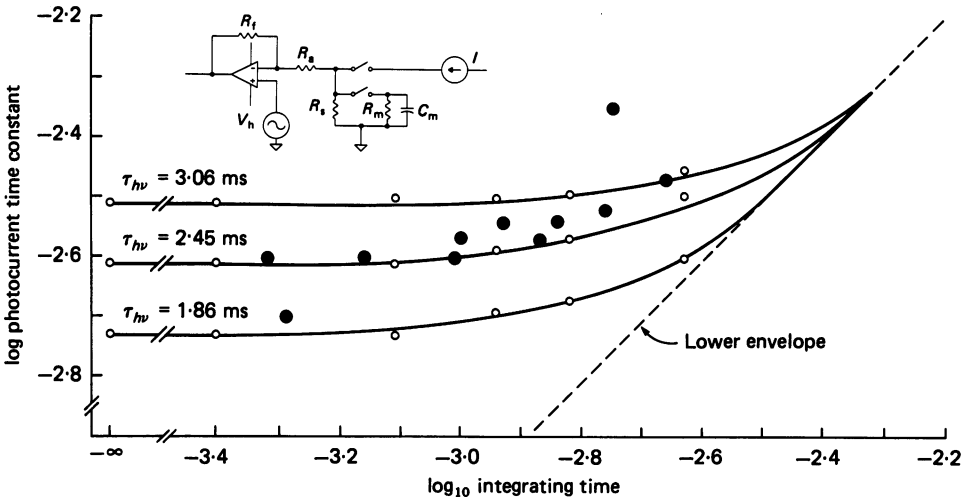

Fig. 11. Filled circles show the time constant of the exponential curve fitted by least squares to the latter two-thirds of the voltage clamp photocurrent of eleven rods stimulated with intense flashes, as in Fig. 10. These time constants are plotted as a function of the clamp integrating time (data in columns 8 and 14 of Table 1). The small open symbols represent measurements made with a model rod (inset) having capacitance $C_m = 30$ pF, resistance $R_m = 1$ GΩ, arranged to have the integrating time given by the abscissa by varying the 'access resistance', R_a. The model rod was driven with an exponentially decaying input current that had one of three time constants: 1·86, 2·45, or 3·06 ms, to simulate three different idealized photocurrents. (Inset: R_s represents the gigaseal resistance, 1–5 GΩ, and R_f, the feed-back resistor in the amplifier.)

A second argument supporting the hypothesis that the 2·8 ms mean photocurrent rise under voltage clamp owes to a limitation in the transduction mechanism can be made by comparing the clamp settling time of each rod with its voltage clamp photocurrent time constant. This comparison is made in Fig. 11. As a measure of the clamp settling time we chose the 'integrating time', which is defined as the integral of the transient component of the voltage clamp response to a 10 ms command step, divided by the maximum transient excursion. This definition obviates problems that have to do with the finite rise of the response to a command step in some cases, which owed to bandwidth limitations and perhaps distributed capacitance. The filled symbols in Fig. 11 show the time constants of the exponential curves fitted to the

voltage clamp photocurrents of eleven rods, as shown in Fig. 9. If the photocurrent time course is determined by the light-driven gating function and not by a limitation of the recording system, for the faster clamp settling times, the voltage clamp photocurrent time constant should become independent of the settling times. The data correspond roughly with this expectation, but leave some doubts. To settle these doubts, we constructed a model rod, and simulated the experiment, deriving the three curves shown along with the data. Each curve represents the time constant of the best-fitting exponential to a simulated photocurrent for a model rod having 30 pF capacitance and a recording integrating time given by the abscissa; the small open symbols represent actual measurements, and the lines represent interpolation. A simple way to interpret these curves is this. When the clamp settling time is much faster than the rising phase of the input current pulse, then the theoretical curve is flat; when the clamp settling time is much slower than the current response, the observed step response will be determined entirely by the integrating time. From this analysis, we conclude that the gating shut of the light-sensitive conductance of the salamander rods at *ca.* 22 °C is limited by a process that has an effective time constant of 2·5 ms.

We now summarize our results on the kinetics of the photocurrent in a graph that shows how maximal photocurrent velocity depends on flash intensity, analogous to the analysis of Penn & Hagins (1972, Fig. 10). For orientation, as an inset in the upper left of Fig. 12 are shown the amplitude saturation functions for the two rods of Figs 1–3: the filled squares represent the voltage clamp data of the rod of Fig. 2; the open squares the current clamp data of the rod of Fig. 3*B*. The continuous line is the 'independence' saturation function of Lamb *et al.* (1981), $J/J_{max} = 1-\exp(-kI)$, where I is the number of isomerizations; the dashed line is the hyperbolic saturation function $J/J_{max} = I/(I+k)$. The data points traversing the entire range of Fig. 12 give the maximal photocurrent velocities for the rods of Table 1 as a function of fraction rhodopsin isomerized. To obtain these data, each digitized photocurrent record was normalized, numerically differentiated, and the maximal value of the derivative in units (fraction maximal photocurrent) per second recorded. To the left, the open and filled squares of Fig. 12*B* give the maximal velocities for the same two sets of responses whose amplitude saturation functions are presented in the upper inset, Fig. 12*A*. For flash intensities above *ca.* $10^{-5.5}$ fractional isomerization, we averaged data of all the rods stimulated at each intensity: the open circles are the average maximum velocities of free cells (recorded with suction electrode only) or cells recorded under current clamp; the filled circles represent the averages of the maximum velocities of rod stimulated under voltage clamp. Error bars are 90% confidence intervals. Points with no error bars are isolated observations.

Several features of the photocurrent velocity saturation function of Fig. 12 deserve comment. First, below about $10^{-7.5}$, velocity linearity obtains as a consequence of the linearity of the complete photocurrent waveform, a linearity which has been established in many other studies (e.g. Lamb *et al.* 1981; Baylor & Nunn, 1986). Our results are consistent with velocity linearity also obtaining between $10^{-7.5}$ and 10^{-7} fractional isomerization (*ca.* 600 isomerizations for our average rod). Secondly, the maximal photocurrent velocity continues to increase with flash intensity for about 4 log units above 10^{-7} fractional isomerization. The rate of increase of maximal

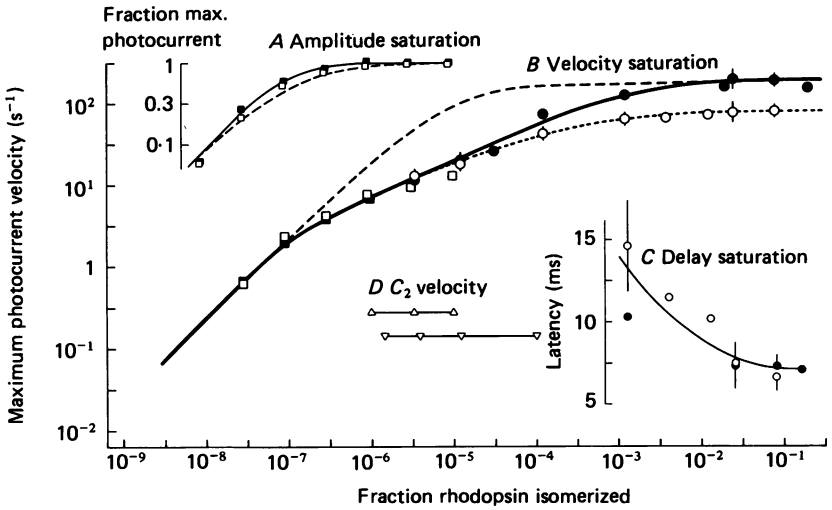

Fig. 12. In *A* the inset in the upper left shows amplitude saturation functions for the two rods of Figs 1–3, the filled symbols referring to photocurrents obtained under voltage clamp, the open symbols to photocurrents recorded under current clamp. Each point represents the fraction of maximal photocurrent produced by a flash producing the fractional isomerization given by the abscissa. The continuous line is the exponential saturation function of Lamb *et al.* (1981); the dashed line, hyperbolic saturation. In *B* the filled symbols associated with the thickened continuous line and the open symbols associated with the closely dashed line traversing the entire graph represent the maximal photocurrent velocities of voltage-clamped and non-voltage-clamped rods respectively. Photocurrent velocity was computed by differentiating the normalized photocurrents. The filled squares in the lower portion of the velocity saturation function (from *ca.* 10^{-8} to 10^{-5} fractional isomerization) are derived from the voltage-clamped photocurrents of the rod of Figs 1 and 2; the open squares are derived from the photocurrents of the rod of Fig. 3*B*, obtained under current clamp. The filled circles represent the average maximum photocurrent velocity of cells recorded under voltage clamp; the open circles, from non-clamped rods. Error bars are 90% confidence intervals for the mean maximal photocurrent velocities of between four and ten different cells stimulated at the given flash intensity. The coarsely dashed line is a hyperbolic saturation function. The continuous and finely dashed curves were drawn by eye through the data. The open and filled circles are all derived from rods identified in Table 1. In *C* the inset in the lower right shows the latency (defined in text) of the photocurrent as a function of flash intensity in the intensity region where the photocurrent velocity has apparently reached saturation. Filled symbols, data from voltage-clamped rods, open symbols, data from non-clamped cells. Error bars 90% confidence intervals. *D*, the triangles represent the maximal velocity of the C_2 component of membrane current described in Fig. 13 (△) and Fig. 14*D* (▽) respectively. The maximal velocity is defined as the reciprocal of the time constant of the best-fitting exponential, as shown in Figs 13 and 14.

velocity over this range is definitely not a linear function of light, however, being reasonably approximated over much of the range by about a 5-fold increase for each decade of increasing light intensity. For reference, the dashed line shows a hyperbolic velocity saturation function. Thirdly, the current clamp (or free cell) maximal photocurrent velocities begin to separate at about 10^{-5} fractional isomerization from the voltage clamp maximal velocities, reaching a very reliable separation of about

2·5-fold. Fourthly, above about $10^{-2.5}$ fractional isomerization, the maximal photocurrent velocities (regardless of clamp condition) reach highly reliable saturation limits. For the voltage clamp data this corresponds to a velocity of *ca.* 200 s^{-1}.

A final point concerns the 'latency' of the photocurrent in the region of intensities over which the velocity is saturated. For voltage clamp photocurrents produced by

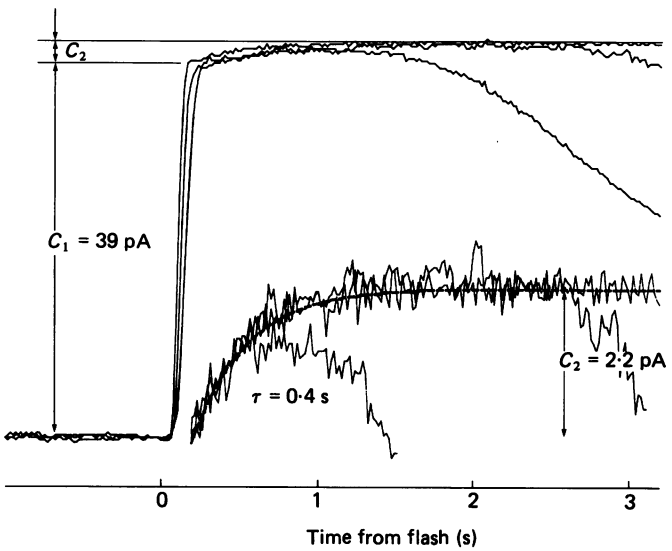

Fig. 13. Evidence for a light-insensitive ionic component of outer segment membrane current. Traces are average photocurrents recorded from outer segment of a rod with suction electrode in response to 22 ms, 500 nm flashes isomerizing $10^{-5.52}$, $10^{-5.02}$ and $10^{-4.52}$ of the rhodopsin. Each record shown is the average of fifteen interleaved flash responses. The lower inset shows the upper portion of the average photocurrents magnified 8-fold; in this inset, the response to the most intense flash is in its true position on the time axis, but the responses to the two less intense flashes have been translated leftwards by 100 and 230 ms respectively. An exponential curve has been fitted by least squares to the non-light-sensitive component: it has a time constant of 0·4 s. The amplitude excursion of the non-light-sensitive component, C_2, was estimated to be 2·2 pA. Rod u of Table 2.

flashes that cause velocity saturation we defined the latency as the intersection of the best-fitting exponential with the time axis (see Fig. 9) for the most intense flash response of a cell. For responses to less intense flashes, the latency was defined as the latency to the most intense, plus the temporal displacement for optimal coincidence of the velocity-saturated photocurrents. For free cells and current-clamped cells we defined the latency as the intersection with the time base of a straight line fitted to the segment of the photocurrent with maximal velocity. Where data of both recording modes were available on the same rod, these definitions were found to agree. Latencies so estimated are presented in Fig. 12*C*, i.e. the inset in the lower right-hand section of Fig. 12. Although the present set of results do not make an unequivocal case, it appears that photocurrent latency continues to decrease as a function of light intensity over a log unit after maximal photocurrent velocity has reached saturation.

A light-insensitive component of outer segment membrane current

An accurate accounting of salamander outer segment flash photocurrent requires the inclusion of a small component of current which is not light sensitive. An analogous component of outer segment membrane current in toad rods has been

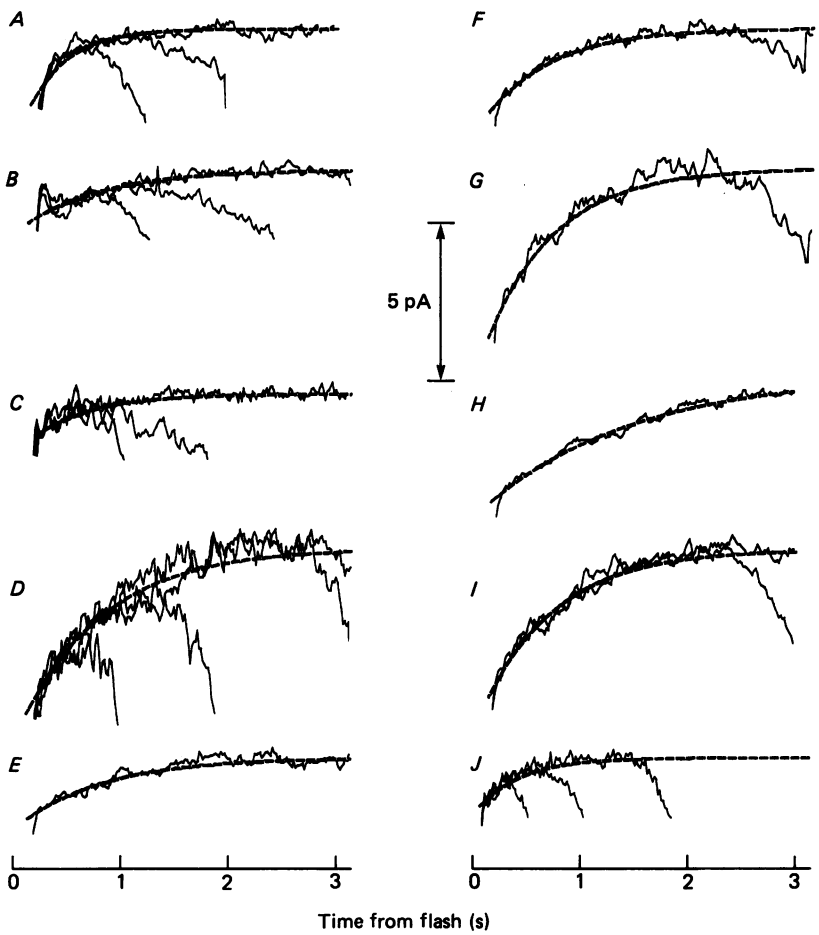

Fig. 14. The C_2 component of outer segment membrane current from ten additional rods. The procedure followed for recovering C_2 was the same as that described for the rod of Fig. 13. Here, however, C_1, the light-sensitive component of current, has been omitted. Table 2 gives additional information for each of the rods whose C_2 component is shown in this Figure. The data of the rod shown in *G* were obtained under voltage clamp. The data shown in *J* were obtained from a rod in Ringer solution containing 5 mM-Ca^{2+}; for this cell, the time base has been contracted 4-fold (i.e. 1 s on the abscissa represents 4 s for this cell.

identified as the decay of an Na–Ca exchange upon blockage of the inward leak of Ca^{2+} through the light-sensitive conductance (Yau & Nakatani, 1984, 1985*a*). Figure 13 shows the way in which this current component can be separated from the light-sensitive current proper. In the experiment the outer segment photocurrent was

measured with a suction electrode and 45 flashes producing $10^{-5.52}$, $10^{-5.02}$ and $10^{-4.52}$ fractional isomerization were interleaved. The fifteen photocurrent responses to each flash were averaged, and the results plotted on a common time base. As expected from Fig. 12, these flashes produce photocurrents with reliably different velocities over most of their trajectory. However, at the top of the responses is a small component of current, labelled C_2, whose time course does not depend on flash intensity. This component is better revealed in the lower insert, where the upper segment of each trace has been amplified 8-fold; for the responses to the two lesser intensity flashes, the curves have been translated to the left 100 and 230 ms,

TABLE 2. Kinetic parameters of light-insensitive component of outer segment membrane current

Rod	Figure	Flash ($\log_{10}$ (fraction isom.))	N	$J_{C_1,\max}$ (pA)	$J_{C_2,\max}$ (pA)	C_1/C_2	τ_{C_2} (s)	Comment
u	13	−5·5, −5·0, −4·5	15	39	2·2	17·7	0·40	—
v	14*J*	−5·5, −5·0, −4·5	22	11	1·6	7·1	1·70	5 mm-Ca^{2+}
w	14*A*	−5·5, −5·0, −4·5	5	35	2·6	13·5	0·36	—
x	14*B*	−5·5, −5·0, −4·5	5	50	1·7	29·4	0·74	—
y	14*C*	−6·0, −5·5, −5·0	11	39	1·3	30·0	0·57	—
g	14*D*	−5·9, −5·6, −4·9, −3·9	4	45	5·3	8·5	0·78	—
p	14*E*	−4·9	6	30	2·0	15·0	0·81	—
q	14*F*	−4·9	9	33	2·7	12·2	0·63	—
z	14*G*	−5·0	8	68	5·4	12·6	0·63	Voltage clamped
*	14*H*	−5·0	8	32	3·9	8·2	1·38	—
†	14*I*	−5·0, −4·5	8	54	5·7	9·5	0·68	—

Data from eleven rods from which a light-insensitive component of outer segment of membrane current was recovered. N is the number of repetitions of each flash intensity averaged to obtain the curves shown either in Fig. 13 or 14. Column labelled $J_{C_1,\max}$ gives the magnitude of the light-sensitive component of current; column labelled $J_{C_2,\max}$, the magnitude of the light-insensitive component. The next column gives the ratio of these, C_1/C_2. The second-from-last column gives the time constant of the exponential fit to C_2 by a least-squares procedure. Some of the rods are also listed in Table 1, as indicated by identifying letter.

respectively, for optimal visual coincidence. An exponential curve was fitted to the data by least squares analysis; the time constant is 0·4 s. If the exponential fit to the C_2 component is extrapolated to the time when the light-sensitive component of current (identified as C_1 in Fig. 13) apparently ends, it is found to have a maximal excursion of 2·2 pA.

We have performed the same experiment on nine additional rods. The C_2 component of current from each of these rods is shown on a common scale in Fig. 14. Additional information about the experiments is provided in Table 2. Important from the perspective of the present study is that the C_2 component of current has an amplitude and time course that are not dependent on light, and whose magnitudes and time course are such as to produce negligible effect on the conclusions we draw here about the dominant phase of the photocurrent. We emphasize this conclusion by plotting the maximum velocity of the C_2 component of two rods on the velocity *vs.* flash-intensity map in Fig. 12*D*. We note that we have observed the C_2 component of outer segment membrane current in the photocurrent of most of the cells of this study, but that reliable estimates of its kinetic parameters under normal

conditions usually require averaging about ten stable photocurrents to a given saturating flash intensity. In particular, we have observed C_2 under voltage clamp at the resting potential (e.g. Fig. 14*G*), which makes it unlikely that the reversal potential (if it exists) of the component in the dark is near the resting potential. In closing, we note an additional bit of evidence consistent with the notion that the C_2 component represents the decay of an Na–Ca exchange current: when external Ca^{2+} is raised, the absolute magnitude of the current is increased, and its time course slowed (Fig. 14*J*).

DISCUSSION

When a rod outer segment held in a suction electrode is stimulated with a light flash, the electrode records membrane current, called throughout this paper simply 'photocurrent'. Three components of photocurrent can be distinguished: (1) light-sensitive ionic current, (2) displacement current and (3) light-insensitive ionic current. Although the principal goal of this investigation has been to re-examine in the light of recent developments in the field of phototransduction the kinetics of decrease in light-sensitive current, we have found it necessary to examine to a certain extent the two other components of outer segment photocurrent in order that our characterization of the light-sensitive current be secure.

Light-insensitive ionic current

Yau & Nakatani (1984, 1985*a*) in experiments on toad rods, first identified a small component of light-insensitive outer segment membrane current very similar to the C_2 component of our experiments (Figs 13 and 14) as the decay of an Na–Ca exchange current. The present results provide some quantitative information about this current component in another amphibian species. The mean C_2 current magnitude of the rods of Table 2 is 6·4% that of the mean light-sensitive current and has a mean time constant of 0·70 s in Ringer solution having 1 mM-Ca^{2+}, as compared to the 6–7·5% and 0·4 s mean values reported by Yau & Nakatani (1985*a*) for toad rods.

Another interesting quantity that can be derived from our measurements of C_2 is f_{Ca}, the fraction of the light-sensitive current carried by Ca^{2+}. It can be deduced that f_{Ca} is equal to twice the exchange current divided by the total light-sensitive current or, in the terms of Table 2, $f_{Ca} = 2J_{C_2}/J_{C_1}$ (see Yau & Nakatani, 1985*a*). From the data in Table 2 we estimate that on average 12·8% of the light-sensitive ionic current is carried by inward leak of Ca^{2+}. A notable feature of our sample rods is that f_{Ca} varies from 6·7 to 24%. We speculate that this 4-fold variation results from differences amongst these rods in resting membrane potential, $[Na^+]_i$ and $[Ca^{2+}]_i$.

Displacement current

An expression relating light-evoked outer segment displacement current i_c to velocity of light-sensitive current can be derived as follows:

$$\left.\begin{aligned} i_c/J_{h\nu,\max} &= C_{os}(dV/dt)/J_{h\nu,\max} \\ &= C_{os}(dV/dJ)(d\bar{J}_{h\nu}/dt) \\ &= C_{os}R(d\bar{J}_{h\nu}/dt). \end{aligned}\right\} \quad (6)$$

Here $J_{h\nu}$ is the light-sensitive current, $J_{h\nu,\max}$ the maximum of the latter, $\bar{J}_{h\nu}$ the normalized light-sensitive current, C_{os} the outer segment capacitance, and $R = dV/dJ$, the instantaneous V–I slope. Equation (6) says that the ratio of the displacement current produced by a flash of a given intensity to the maximum light-sensitive current is the product of the velocity of the light-sensitive current and the outer segment capacitance and the instantaneous slope resistance of the whole rod. For any specific set of parameters R and C_{os}, eqn (6) combined with the data of Fig. 12 yields a prediction about the flash intensity that will produce a given magnitude capacity current. For example, for the representative values $C_{os} = 15$ pF, and $R = 1000$ MΩ, it is predicted that light-evoked outer segment displacement current will be less than 10% of the maximum light-sensitive current if $d\bar{J}_{h\nu}/dt < 6{\cdot}7$. From Fig. 12, we see that this condition will be met for flashes producing fractional isomerization less than about 4×10^{-6}. Consistent with this latter estimate, we found that the maximum photocurrent velocity of voltage-clamped rods was reliably higher than that of non-voltage-clamped rods for flashes producing in excess of *ca.* 10^{-5} fractional isomerization.

If, even when a rod is not voltage clamped, the velocity of the light-sensitive current proper continues to increase with flash intensity in the intensity range ($> 10^{-5}$ fractional isomerization) where capacitative loading becomes significant, then providing voltage-activated conductances are activated slowly relative to hyperpolarization rate (Baylor *et al.* 1984; Bader, Bertrand & Schwartz, 1985; Owen, 1987) for very intense flashes the photovoltage should approach a velocity limit set by $R \times C$, where R is the instantaneous slope resistance of the membrane at rest and C is the total capacitance of the rod. Correspondingly, the velocity of the photocurrent of an outer segment in a suction electrode can be expected to approach a limiting velocity set by the same product $R \times C$. Comparison of τ_{cc}, the time constant of an exponential fit to the non-voltage-clamped photocurrent (Table 1, column 14), with the product $R \times C$ (columns 6 and 7) for the nine rods (rows a, c, i, k, l, o, q, r and s) for which pertinent data are available shows reasonable agreement between observation and expectation: the mean value of the percentage error statistic $100 \times |(\tau_{cc} - RC|)/[(\tau_{cc} + RC)/2]$ is 19%, and 14·7% if the data of rod c, which had a 55% error, is excluded from the mean.

Light-sensitive ionic current

Here we examine the constraints put on the theory of phototransduction imposed by the salient features of the light-sensitive current response to intense flashes. These features are the following: (1) *velocity saturation*, an ultimate limit of *ca.* 200 s^{-1} to the rate of change of the normalized light-sensitive current induced by flashes producing fractional isomerizations greater than 0·001 (Fig. 12*B*); (2) *delay*, an interval of time exceeding 7 ms preceding acquisition of the maximal (saturated) velocity (Fig. 9); (3) *translation invariance*, a relation between light and time such that for fractional isomerization between 0·001 and 0·1 responses of the same shape occur at earlier times with more intense flashes (Fig. 8); (4) *delay saturation*, an ultimate limit of about 7·5 ms to the delay in the responses to the most intense flashes (Fig. 12*C*). A satisfactory theory of transduction must account for these four features of the light-sensitive current.

The central result of this investigation was the determination of limits of the maximal velocity of the photocurrent evoked by intense, brief flashes (Fig. 12*B*). In the absence of voltage clamp, the observed velocity limit is apparently determined by the passive electrical properties of the rod membrane. Penn & Hagins (1972) similarly concluded that the maximal velocity of the photocurrents of rat rods measured with extracellular electrodes were rate-limited by passive electrical properties. Under voltage clamp, however, we observed a distinct velocity saturation limit (Fig. 12*B*, ●), higher than that measured without clamp (Fig. 12*B*, ○), which we concluded arises in the phototransduction mechanism (i.e. in the events initiated by photon absorption and ending in closure of the light-sensitive conductance) and not in passive membrane properties.

Phototransduction theories (Penn & Hagins, 1972; Baylor, Hodgkin & Lamb, 1974) have been proposed that posit a linear relation between photoactivated visual pigment and the rate of release of an internal excitatory transmitter. These theories correctly predict photoresponse velocity to increase with flash intensity over the range of intensities that produce response amplitude saturation. However, they incorrectly predict photocurrent velocity under voltage clamp to increase with flash intensity over the entire range of isomerizations and delay to decrease correspondingly. In contrast, as we now discuss, the cyclic GMP cascade theory of transduction incorporates reactions that could be the basis of the velocity- and delay-saturation phenomena reported here.

Equation (7) is a chemical representation of the cyclic GMP cascade (e.g., see Stryer, 1986; Lamb, 1986; Pugh & Cobbs, 1986).

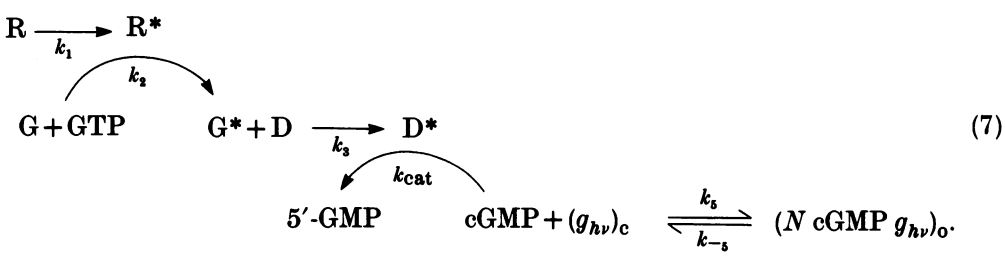

(7)

Five steps of the cascade are identified: (1) conversion of rhodopsin, R, by light into its active form, R*; (2) conversion of G-protein, G, to its active form, G*, by R*-catalysed binding of GTP; (3) conversion of phosphodiesterase, D, to its active form, D*, by the binding of some moiety of G*; (4) D*-catalysed hydrolysis of cytoplasmic cyclic GMP (cGMP); (5) modulation of the amount of the light-sensitive conductance, $g_{h\nu}$, opened and closed by the binding and unbinding respectively of N molecules of cyclic GMP, in a co-operative manner. (The subscripts o and c refer to open and closed.) In this simplified scheme we omit consideration of the inactivation reactions of the first three steps of the cascade, and of the guanylate cyclase reaction which restores free cyclic GMP to its baseline level, on the assumption that these reactions are insignificant in the first 50 ms after an intense flash (see Pugh & Cobbs, 1986 for discussion of the latter point). How might each of the steps in (7) contribute to velocity saturation and delay?

(1) *Rate of activation of rhodopsin, $R \rightarrow R^*$.* This transition is thought to be the conversion of rhodopsin to metarhodopsin II (Meta II; Parkes & Liebman, 1982; Bennett, Michel-Villaz & Kuhn, 1982), which may be taken to be establishment of Meta I $\rightleftharpoons$ Meta II equilibrium at room temperature. This reaction cannot be the basis of velocity saturation, and probably makes only a small contribution to the delay, for the following reasons. First, the time constant of the Meta I $\rightleftharpoons$ Meta II equilibrium reaction at 22 °C in amphibian rods is about 1·3 ms (Baumann, 1978), considerably briefer than the fastest photocurrent. Secondly, this reaction is the initial one (on the time-scale of milliseconds) in the cascade, and must necessarily be subsumed in the greater than 7 ms delay period that precedes the acquisition of maximum photocurrent velocity. In effect, if Meta II is R*, then the production of R* following a 20 μs flash approximates a step function relative to the subsequent events.

(2) *Rate of activation of G-protein.* The activation of G-protein occurs via R* catalysis of GDP–GTP exchange (Fung & Stryer, 1980; Fung, Hurley & Stryer, 1981). It has been estimated that in the presence of cytoplasmic GTP a single molecule of R* per disc can activate 500–1000 molecules of G-protein per second (Liebman & Pugh, 1982; Vuong & Stryer, 1984). These latter numbers require that it takes on average 1–2 ms for an arbitrary R* molecule at the lowest flash level to encounter an inactive molecule of G-protein and catalyse its binding of GTP. However, it seems unlikely that G-protein activation is the basis of the photocurrent velocity limit, since if it were there would be no basis for the delay period, given an $R \rightarrow R^*$ transition of 1·3 ms.

It seems plausible, however, that G-protein activation is the basis of *delay saturation*. The reason is that the level of fractional isomerization at which delay saturation occurs (Fig. 12*C*) corresponds approximately to the ratio of G-protein to rhodopsin, about 0·1. One would expect that the speed of subsequent reactions of the cascade could not be increased by increasing the fraction of rhodopsin isomerized, once there is one R* molecule activated for every molecule of G-protein, providing the time it takes for R* to encounter an inactivated G-protein is brief relative to subsequent events. Although the existence of delay saturation at about 0·1 fractional isomerization may thus be explained, the magnitude (7 ms) of the saturated delay cannot be explained without postulating some intervening delay steps not represented in eqn (7). (See below and Appendix.)

(3) *Rate of activation of phosphodiesterase.* At present the shortest time constant reported for the total activation of phosphodiesterase by a brief, intense flash (isomerizing 0·1–0·2 rhodopsin) is 50–100 ms (Liebman & Evanczuk, 1982). Mathematical simulation (see Appendix) has led us to conclude that a time constant as long as 50 ms for this step of the cascade is definitely incompatible with our results. The biochemical data bearing on this issue were obtained from a suspension of rod membranes whose phosphodiesterase activity was assayed with a pH electrode or dye. It is possible that the delay from the flash to the appearance of maximal phosphodiesterase activity was limited by recording apparatus bandwidth. It seems reasonable to believe that activation of phosphodiesterase by G* takes place on the same time-scale (a few milliseconds) as activation of G-protein by R*. None the less,

at present the apparent sluggishness of the activation of phosphodiesterase by G-protein poses a serious impediment to explaining our results in terms of the cyclic GMP cascade.

(4) *Rate of removal of cyclic GMP from the rod cytoplasm.* In the Appendix it is shown that a lower bound on the rate of removal of free cyclic GMP from the cytoplasm is given by the ratio V_{max}/k_m, where V_{max} is the maximum hydrolytic velocity (units: M s^{-1}) attainable by the total phosphodiesterase of the outer segment, and k_m is the cyclic GMP concentration that produces half-maximal velocity for a fixed complement of activated phosphodiesterase. Furthermore, it is shown that under conditions where all the phosphodiesterase of the outer segment is activated as a step with a pure delay, and where the rate constant k_{-5} in eqn (7) greatly exceeds V_{max}/k_m, that the light-sensitive current can be predicted to decline exponentially with a time constant $\tau = k_m/(NV_{max})$, where N is the number of cyclic GMP molecules required to open the cyclic GMP-gated conductance. Insertion in the latter expression of values taken from published biochemical data (see Appendix) yield estimates of the time constant τ of 0·8–2 ms. Thus removal of cyclic GMP from the cytoplasm is a plausible mechanism of photocurrent velocity saturation.

(5) *Rate of closure of the light-sensitive, cyclic GMP-gated conductance.* According to the current cyclic GMP cascade theory of transduction, the unbinding of cyclic GMP from the light-sensitive conductance, $g_{h\nu}$, suffices to close it. Single-channel measurements could in principal provide estimates of the microscopic rate constant for this gating, but such data are not presently available and their interpretation will be conditioned by the fact that the unitary conductance is too small in Ringer solution containing normal amounts of divalent cations to resolve single-channel events (Fesenko *et al.* 1985; Haynes, Kay & Yau, 1986; Zimmerman & Baylor, 1986). Power spectra of outer segment light-sensitive noise may provide another independent estimate of the rate(s) of the cyclic GMP-dependent gating, although the partial blocking effects of divalent cations necessarily complicates interpretation of such data obtained in normal Ringer solution. Bodoia & Detwiler (1984), Gray & Attwell (1985) and Matthews (1987) have reported a light-dependent component of noise with a Lorentzian power spectrum and a corner frequency, f_c, of 100–300 Hz. For a two-state channel the corner frequency satisfies $2\pi f_c = (a+b)$, where a and b are the rate constants for opening and closing respectively of the channel under a defined steady-state condition. Both Bodoia & Detwiler (1984) and Gray & Atwell (1985) note that f_c is independent of illumination level, consistent with the conclusion that for all conditions examined the rate of closing (here, equivalent to the unbinding of at least one cyclic GMP molecule) is much faster than the rate of opening. It follows that the mean open time of the channel is $1/(2\pi f_c)$, which in salamander Gray & Attwell (1985) estimate to be 2 ms and in frog Bodoia & Detwiler (1984) estimate to be 750 μs. The former is reasonably close to the 2·5 ms decay limit of the voltage clamp photocurrent, and thus provides a second plausible mechanism of photocurrent velocity saturation.

We summarize our discussion of possible explanations afforded by the cyclic GMP cascade of the features (velocity saturation, delay, translation invariance and delay saturation) of the voltage clamp photocurrent responses to intense flashes by showing two sets of theoretical photocurrents (Fig. 15*C* and *F*) that reproduce these

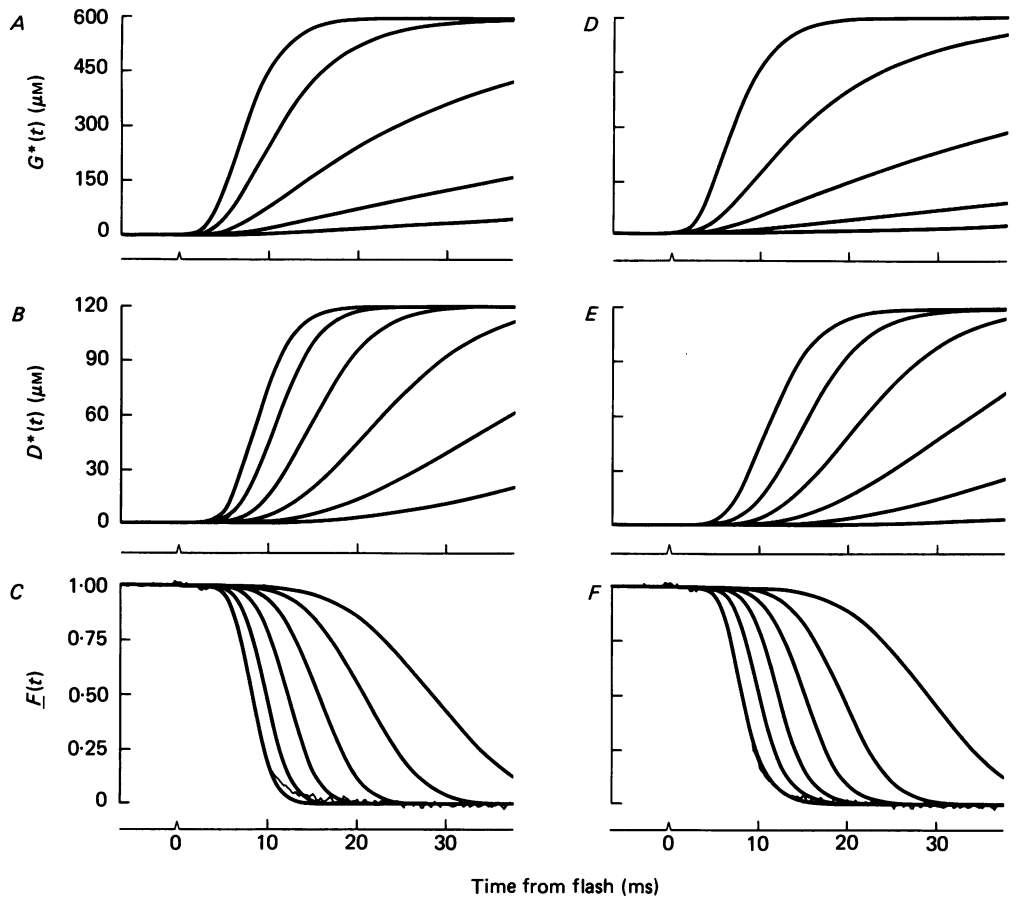

Fig. 15. Flash responses (heavy lines) generated by two different representations of the cyclic GMP cascade theory. One representation generated the curves of *A*, *B* and *C*; a second representation generated the curves of *D*, *E* and *F*. The thin, noisy trace in *C* and *F* is the mean normalized voltage-clamped photocurrent of rods, b, i, l, o, r and s of Table 1, resulting from stimulation with a flash isomerizing 7·6% of the rhodopsin. The photocurrent records were translated 0, 0, 0·6, 1·0, 0·6 and 1·2 ms respectively before averaging. The representations of the cyclic GMP cascade employed were based upon eqn (7), as described in the Appendix. Each of a large set of representations was evaluated by the degree to which the photocurrent it generated fitted, by eye, the mean photocurrent (noisy trace). In *A*, *B*, *D* and *E* the left-most curves are the time courses of the intervening variables activated G-protein, $G^*(t)$, and activated phosphodiesterase, $D^*(t)$, corresponding to the two curves in *C* and *F* fitted to the data trace. To generate the theoretical curves in the panels other than the left-most ones the single rate constant k_{20} (see Appendix) was decremented in approximately geometric fashion. For the curves of panels *A–C* the values assumed by $1/k_{20}$ were 1·5, 6, 25, 100, 400 and 1600 ms; for the curves of panels *D–F*, the values of $1/k_{20}$ were 2·0, 12·5, 50, 200, 800 and 6000 ms. The other rate constants of the two theoretical representations remained fixed; they are given in Tables 3 and 4 in the Appendix.

phenomena. The theoretical curves of Fig. 15*C* were generated by a representation in which photocurrent velocity saturation is produced by the maximal phosphodiesterase activity; the rate of unbinding of cyclic GMP from the light-sensitive conductance and its closure are assumed to be about four times faster, and not rate-limiting. The theoretical curves of Fig. 15*F* were generated with a representation in which maximum photocurrent velocity is rate-limited by the unbinding of cyclic GMP and closure of the light-sensitive conductance. Although the latter theory can be seen to fit the average velocity-saturated photocurrent better, the necessity of assuming in the latter case a maximal phosphodiesterase activity ten times that expected from biochemical data shifts the balance in favour of the former theoretical explanation. The two hypotheses predict substantially different maximal photocurrent velocities in the presence of exogenous, infused cyclic nucleotides.

The effort to construct a representation of the cyclic GMP cascade that could account quantitatively for the salient features of our data yielded two conclusions about the cascade not anticipated from direct analysis of the photocurrent data. The first is that approximately four first-order delay steps of magnitude about 2 ms must be hypothesized to occur after R* production and before the event that produces velocity saturation. It seems natural to suppose that these delay steps may represent intermediates in the activation of G-protein and/or phosphodiesterase. The second, and perhaps more interesting conclusion, is that computational realizations of the theory that reproduce the delay and velocity saturation generate the translation invariance phenomenon in a natural way, viz. by variation in the rate constant governing the time course with which R* activates G-protein. In Fig. 15*C* and *F* the families of simulated photocurrents were generated by approximately geometric decrements in this rate constant. In short, the entire functional dependence of the excitatory side of the cascade on f_I, the fraction of rhodopsin isomerized, is captured in this single rate constant, which we may label $k_{20}(f_I)$ (see Appendix).

A physical theory of this rate constant can be developed from the hypothesis that each R* activates a complement of G-protein by lateral diffusion within the disc membrane (Liebman & Pugh, 1981). The rate constant $k_{20}(f_I)$ would then represent the reciprocal of the mean time $\tau_D(f_I)$ with which each R* activates its complement of G-protein, for a given areal density of isomerized rhodopsin. First passage time theory (Szabo, Schulten & Schulten, 1980) gives an analytical expression for the mean time τ_D for exhaustion by an enzyme of an initially limited supply of substrate on a finite two-dimensional disc, when the reaction rate is diffusion-limited. A first-order approximation is $\tau_D = A_{R^*}/D_{eff}$, where $A_{R^*} = A_R/f_I$, $1/A_R$ is the areal density of rhodopsin, and D_{eff} the effective diffusion constant of the encounter. Thus,

$$\left.\begin{aligned}\tau_D(f_I) &= A_R(1/f_I)/D_{eff} \\ &= (40\times10^{-6})(1/f_I)\ \text{s}\end{aligned}\right\} \quad (8)$$

assuming $1/A_R = 25000$ rhodopsins/μm^2, and $D_{eff} = 1{\cdot}0\ \mu m^2/s$, with $0{\cdot}5\ \mu m^2/s$ being the lateral diffusion coefficient of rhodopsin (Poo & Cone, 1974; Liebman & Entine, 1974).

Equation (8), predicted purely by the physics of lateral diffusion, can be compared with the delay or latency data of Fig. 12*C*. There the light-sensitive component Δt of the delay of the velocity-saturated photocurrent is shown to be described by the

purely empirical relation (continuous line) $\Delta t = (120 \times 10^{-6})(f_I)^{-0.6}$ s. For the theoretical representation of the cascade that generated Fig. 15*A–C*, over the range of $k_{20}(f_I)$ for which translation invariance is obeyed, the relation $\Delta t = (36 \times 10^{-3})(k_{20})^{-0.6}$ s obtains. This relation can be verified by plotting the time shift between the theoretical curves as a function of k_{20} on double-log co-ordinates. Setting these two expressions for Δt equal to one another gives the relation

$$1/k_{20}(f_I) = (76 \times 10^{-6})(1/f_I) \text{ s}, \tag{9}$$

which bears a notable resemblance to eqn (8), predicted from the physics of rhodopsin lateral diffusion and the hypothesis that this diffusion constitutes a rate-limiting step in G-protein activation.

APPENDIX

A mathematical representation of the cyclic GMP cascade for the first 50 ms of the light response

This Appendix has two purposes. The first is to represent the cyclic GMP cascade, given as a chemical scheme in eqn (7) of the Discussion, as a system of differential equations. The second is to explain how solutions of this system reproduce the principal qualitative features of intense-flash voltage clamp photocurrents, viz. velocity saturation and approximate translation invariance at very high fractional isomerizations.

Variables and rate equations

The time-dependent variables of the system are these:

R^* = [photoactivated rhodopsin];
G^* = [activated G-protein];
D^* = [activated phosphodiesterase];
S = [cyclic GMP]
$F = [g_{h\nu}]_{open}/[g_{h\nu}]_{tot}$, fraction $g_{h\nu}$ open.

All concentrations are referred to the rod cytoplasm. Because the data to be explained result from flash intensities that produce many thousands of isomerizations, cytoplasmic diffusion is considered to be adequate for producing isotropy of [cyclic GMP] throughout the outer segment.

Our differential equation representation is the following:

$$dR^*/dt = k_1(f_I R_{tot} - R^*) \qquad \text{R* production,} \tag{A 1}$$

$$dG^*/dt = k_2(f_I)(R^*/f_I R_{tot})(G_{tot} - G^*) \qquad \text{G* production,} \tag{A 2}$$

$$dD^*/dt = k_3 G^*(D_{tot} - D^*) \qquad \text{D* production,} \tag{A 3}$$

$$dS/dt = -k_{cat} D^* S/(S + k_m) + K_c \qquad \text{cyclic GMP modulation,} \tag{A 4}$$

$$dF/dt = k_5 S^N(1 - F) - k_{-5} F \qquad g_{h\nu} \text{ regulation.} \tag{A 5}$$

This representation of the cyclic GMP cascade contains some apparently arbitrary choices (e.g. representing the conductance, $g_{h\nu}$, in a *two-state* rate theory (eqn (A 5)

with ligand gating strictly co-operative.) The guiding principles in the selection of the mathematical representation of the cyclic GMP cascade were parsimony (Occam's razor), and explicit incorporation of relevant biochemical measurements. The inactivation reactions of the first three steps of the physiological cascade are considered negligible in the first 50 ms after an intense flash (e.g. see Pugh & Cobbs, 1986).

Relation to voltage clamp photocurrents

To compare measured voltage clamp photocurrents with theory a normalized variable $\underline{F}(t) = F(t)/F(0)$ is defined, where $F(0)$ is the fraction of the light-sensitive conductance open in the dark immediately before a flash. Under reasonable assumptions about the stationarity of ionic gradients, $\underline{F}(t) = [J_{h\nu,\max} - J_{h\nu}(t)]/J_{h\nu,\max}$, where $J_{h\nu}(t)$ is the light-sensitive current of the outer segment, and $J_{h\nu,\max}$ its maximum value. Note that $\underline{F}(t)$ is the ordinate in Fig. 15*C* and *F*.

Parameters

Table 3 lists the parameters that must be assigned values in order to solve the system. In so far as it is possible, fixed numerical values were assigned on the basis of published data; references and the logic of the assignments are given along with the values, and explained below. For some parameters specific numerical values could not be assigned, but a range of possible values consistent with published data has been listed. For others no rationale for assignments other than constraints imposed by our data were found.

Initial conditions

Initial values of the five variables must be assigned to integrate eqns (A 1)–(A 5). The terms $R^*(0)$, $G^*(0)$ and $D^*(0)$ were assumed to be negligible before, relative to the values they would assume after, intense flash activation. They were therefore assumed equal to zero; this assumption is an approximation likely to be invalid at low flash levels. The terms $S(0)$ and $F(0)$ can be assigned on the basis of steady-state considerations that exist prior to flash activation.

The steady-state solutions to eqns (A 4) and (A 5) are

$$S = K_c[k_m/(k_{cat}\, D^*)], \tag{A 6}$$

$$F = S^N/(S^N + K_D^N), \tag{A 7}$$

where $K_D = (k_{-5}/k_5)^{(1/N)}$ is the concentration of cyclic GMP that causes 50% opening of the cyclic GMP-gated conductance (Fesenko *et al.* 1985; Yau & Nakatani, 1985*b*; Haynes *et al.* 1986). The value of K_D has been estimated from recordings of isolated patches of salamander outer segment membrane to be 17 μm (Zimmerman, Yamanaka, Eckstein, Baylor & Stryer, 1985) and N to be 3 (Zimmerman & Baylor, 1986). The latter estimate of N was obtained in Ringer solution depleted of divalent cations; estimates from other amphibian membranes in normal Ringer solution give $N \simeq 2$ (Fesenko *et al.* 1985; Yau & Nakatani, 1985*b*). The value of K_c is thought to be only a very small fraction of the maximum light-activated phosphodiesterase activity and thus should be negligible, in the sense that when most or all of the

phosphodiesterase is activated the value S dictated by eqn (A 6) produces no measurable value of F in eqn (A 7) (see Pugh & Cobbs, 1986, for discussion). Our own observations and those of others show that no more than 5–10 % of the cyclic GMP-activated conductance is open in an amphibian rod at rest in the dark (Cobbs & Pugh, 1985; Yau & Nakatani, 1985*b*; Zimmerman *et al.* 1985), and so $F(0)$, the fraction of cyclic GMP-gated conductance open immediately before the flash is

TABLE 3. Parameters of the cyclic GMP cascade

Parameter	Value	Meaning	Reference or comment
f_I	—	Fraction R_{tot} isomerized	Experimental variable
R_{tot}	6 mM	Total [rhodopsin]	Liebman (1972)
G_{tot}	$R_{tot}/10$	Total [G-protein]	Applebury & Chabre (1986)
D_{tot}	$R_{tot}/50$	Total [PDE] (phosphodiesterase)	Applebury & Chabre (1986)
k_1	770 s^{-1}	Meta I$\rightleftharpoons$II equilibration rate	Baumann (1978)
$k_2(f_I)$	—	$h\nu$-dependent G-protein activation rate	See Discussion, Fig. 15
k_3	> 10 s^{-1}	PDE activation rate	Liebman & Evanczuk (1982)
k_{cat}	2000 s^{-1}	PDE turnover number	Baehr, Devlin & Applebury (1979)
k_m	580 μM	PDE Michaelis constant	Barkdoll *et al.* (1986)
K_C	—	Guanylate cyclase rate	Negligible for large f_I
k_{-5}	> 500 s^{-1}	Cyclic GMP 'off rate' from $g_{h\nu}$	See Discussion
N	2–3	Co-operativity index	Zimmerman & Baylor (1986)
K_D	17 μM	K_D of $g_{h\nu}$ for cyclic GMP	Zimmerman & Baylor (1986)

delivered, is assumed to be 0·05. The re-normalized solution $\underline{F}(t) = F(t)/F(0)$ is essentially invariant over changes in $F(0)$, for $F(0) < 0{\cdot}05$. Given $F(0)$ and K_D, $S(0)$ is determined by inverting the eqn (A 7). We note that always for a normal rod, for which $F < 0{\cdot}1$, at steady state in the dark or light, eqn (A 7) can be well approximated by the simpler relation

$$F = (S/K_D)^N. \tag{A 8}$$

Two limiting cases that give exponential photocurrent decay

Suppose that an intense flash activated all the phosphodiesterase in the rod, after a period of pure delay (t_d), i.e. $D^*(t) = D_{tot}\,u(t-t_d)$, where $u(t)$ is the Heaviside step function. The solution to eqn (A 4) subject to these assumptions is

$$S(t) = S_\infty + [S(0) - S_\infty] \exp[-(t-t_d)/(k_m/V_{max})], \tag{A 9}$$

where $V_{max} = k_{cat}\,D_{tot}$. In other words, under these conditions, [cyclic GMP] would relax from its initial value $S(0)$ in the dark to its final value S_∞ given by eqn (A 6) with a time constant k_m/V_{max}. If it be assumed that the equilibrium rate constant of the binding reaction (A 5) is much higher than V_{max}/k_m, then combining eqns (A 8) and (A 9) one obtains

$$F(t) = F(0) \exp[-(t-t_d)/(k_m/NV_{max})]. \tag{A 10}$$

Equation (A 10) implicitly recognizes that after an intense flash F_∞ is a negligible fraction of $F(0)$. Equation (A 10) thus states that if all the phosphodiesterase of the

outer segment were activated as a step with a pure delay t_d after a flash, and if the rate of unbinding of the essential cyclic GMP from the cyclic GMP-dependent conductance is much faster than V_{max}/k_m, then normalized voltage clamp photocurrent would decay with an exponential time course having a time k_m/NV_{max} $= 800\,\mu s$, given the numerical values of Table 3.

It can be reasonably objected that the derivation of eqn (A 10) employed the Michaelis formalism, and that an assumption made in the derivation of that formalism is that substrate greatly exceeds active enzyme concentration. In violation of that assumption is that the concentration of phosphodiesterase referred to the cytoplasm is $120\,\mu M$, whereas $S(0)$, the initial cyclic GMP activity before a flash, is thought to be less than $10\,\mu M$. None the less eqn (A 10) will set a lower bound on the rate of disappearance of cyclic GMP from the cytoplasm, because of a general theorem in enzyme kinetics that shows that k_{cat}/k_m necessarily is a lower bound on the rate constant of association of enzyme and substrate (Fersht, 1977, p. 91). This theorem thus predicts that $V_{max}/k_m = (k_{cat}\,D_{tot})/k_m$ will be the lower limit on the rate of removal of cyclic GMP from the outer segment cytoplasm.

An alternative possibility for the velocity limitation of the voltage clamp photocurrent is suggested by eqn (A 5). The off-rate, k_{-5}, of the cyclic GMP binding reaction that opens the conductance could be rate-limiting for the closure of the light-sensitive conductance by intense flashes. If light-activated phosphodiesterase removes cyclic GMP from the cytoplasm as a step after a delay t_d, then the fraction of light-sensitive conductance open would decay as

$$F(t) = F(0)\exp[-k_{-5}(t-t_d)]. \qquad \text{(A 11)}$$

Equation (A 11) states the rate constant k_{-5} necessarily sets an upper bound on the rate of closure of $g_{h\nu}$, the light-sensitive conductance.

Numerical solution and an expanded representation of the cascade

The system of eqns (A 1)–(A 5) cannot be solved analytically except for limiting conditions such as those just discussed in deriving eqns (A 10) and (A 11). Although analysis of these limiting cases does reveal two distinct mechanisms that may underlie the approximately exponential, velocity-saturated latter phase of the photocurrent, such analysis gives no insight into the other salient features of the intense-flash, voltage clamp photocurrents. In particular, there remains no explanation for (i) the existence of a relatively long 'delay' period between the flash and the foot of the photocurrent, (ii) the saturation and light dependence of the delay, and (iii) the approximate translation invariance of the velocity-saturated portion of the response.

To determine whether the cyclic GMP cascade could explain these salient features of the photocurrent, (A 1)–(A 5) were solved by a fourth-order Runge–Kutta method. Very good reproductions of the dominant phase of the velocity-saturated photocurrents were generated by solutions in which the decay phase was dominated by either k_{-5}, or by k_m/V_{max}, as anticipated from eqns (A 10) and (A 11). However, the form and magnitude of the delay period could not be reproduced without assuming that there exist stages of delay in addition to those expressed in eqns (A 1)–(A 5).

Two steps in the cascade where additional, brief, delays might be expected to occur would be in the $G \rightarrow G^*$ and $D \rightarrow D^*$ transitions. In other words, activation of G-protein might proceed as $G_0 \rightarrow G_1 \rightarrow \ldots G_n = G^*$, where the subscripts represent internal conversions that are not dependent on other time-dependent variables. Likewise, activation of phosphodiesterase might proceed as $D_0 \rightarrow D_1 \rightarrow \ldots D_m = D^*$. A mathematical representation of such delay steps is as follows.

For *G-protein activation*:

$$dG_0/dt = -k_{20} R^* G_0, \tag{A 2.0}$$

$$dG_1/dt = k_{20} R^* G_0 - k_{21} G_1, \tag{A 2.1}$$

$$dG_i/dt = k_{2,i-1} G_{i-1} - k_{2i} G_i, \quad i = 2,\ldots n-1, \tag{A 2.i}$$

$$dG_n/dt = k_{2,n-1} G_{n-1}, \tag{A 2.n}$$

where $G_0(0) = G_{\text{tot}}$, and $G_n = G^*$.

For *phosphodiesterase activation*:

$$dD_0/dt = -k_{30} G^* D_0, \tag{A 3.0}$$

$$dD_1/dt = k_{30} G^* D_0 - k_{31} D_1, \tag{A 3.1}$$

$$dD_j/dt = k_{3,j-1} D_{j-1} - k_{3j} D_j, \quad j = 2,\ldots m-1, \tag{A 3.j}$$

$$dD_m/dt = k_{3,m-1} D_{m-1}. \tag{A 3.m}$$

with $D_0(0) = D_{\text{tot}}$, $D_{\text{m}} = D^*$. Mathematically, eqns (A 2.1)–(A 2.n) and (A 3.1)–(A 3.m) are the equations of low-pass filters. Physically, they could be interpreted as rate equations for internal conversion states of the proteins, G-protein and phosphodiesterase. For example, for G-protein the rate equations could represent GDP release, GTP binding, and conformation change.

Our goal was to find a minimal, plausible representation of the cyclic GMP cascade that accounts for the major qualitative features of the voltage clamp photocurrent data. The strategy for evaluating solutions to the expanded set of rate equations was this. The rate equations (A 1), (A 2.0)–(A 2.n), (A 3.0)–(A 3.m), (A 4) and (A 5) were numerically integrated with a fourth-order Runge–Kutta routine, and each particular solution $F(t)$ compared by eye with the average velocity- and delay-saturated photocurrent (see Fig. 15, left-most curves in panels *C* and *F*). Throughout the present implementation the rate constants k_{2i}, $i > 0$ were kept identical, and likewise the rate constants k_{3j}, $j > 0$, and minimal m and n were sought that provided reasonable approximations to our velocity- and delay-saturated photocurrents. Facilities did not permit an exhaustive search of the parameter space for optimum fits, inasmuch as computation of each solution to the complete set of equations took approximately 1 min. Several sets of parameters were found to give reasonable fits to the average velocity- and delay-saturated photocurrent, two of which are shown in Fig. 15 of the Discussion. The solution of Fig. 15*C* is rate-limited by the rate constant $V_{\text{max}}/k_{\text{m}}$; the solution of Fig. 15*F* is rate-limited by the rate constant k_{-5}. Table 4 shows the particular parameter values of the theoretical curves fitted to the velocity- and delay-saturated photocurrent of Fig. 15*C* and *F*.

A remarkable finding resulted from examination of solutions to the expanded system. Recall that all light intensity dependence of the rate parameters of this

TABLE 4. Cyclic GMP cascade parameters* for curves of Fig. 15

Parameter	Value	Comment
(a) Velocity saturation produced by phosphodiesterase (Fig. 15*A–C*)		
k_{20}	667 s^{-1}	Maximum rate, for $f_I > 0{\cdot}1$
k_{2i}, $i = 1$–4	540 s^{-1}	Three intermediate states
k_{30}	667 s^{-1}	—
k_{3j}, $j = 1,2$	540 s^{-1}	One intermediate state
V_{max}	240 mM s^{-1}	$V_{max} = D_{tot} k_{cat}$
N	3	Co-operativity index
k_{-5}	2000 s^{-1}	—
(b) Velocity saturation produced by off-rate, k_{-5} (Fig. 15*D–F*)		
k_{20}	500 s^{-1}	Maximum rate, for $f_I > 0{\cdot}1$
k_{2i}, $i = 1$–3	435 s^{-1}	Two intermediate states
k_{30}	500 s^{-1}	—
k_{3j}, $j = 1$–3	476 s^{-1}	Two intermediate states
V_{max}	2400 mM s^{-1}	10 times biochemical estimates!
N	2	Co-operativity index
k_{-5}	455 s^{-1}	—

*Parameters not given in this Table are specified in Table 3.

representation of the cyclic GMP cascade equation resides in the single rate constant $k_{20} = k_2(f_I)$. Once a set of parameters that yielded a good fit to the mean velocity- and delay-saturated photocurrent was found, the single rate constant k_{20} was decreased in geometric steps, while all other parameters were kept constant. At each step change in k_{20} a new solution to the system was generated. This is how the family of curves in Fig. 15*A–C* and *D–F* were produced. The approximate translation invariance of the velocity-saturated photocurrent can thus be generated by such cascade representations (Fig. 15*C* and *F*).

This research was supported by NIH Grants EY-02660 and EY-06192. We thank S. Ari, D. Baylor and J. Tanaka for helpful comments.

REFERENCES

APPLEBURY, M. L. & CHABRE, M. (1986). Interaction of photoactivated rhodopsin with photoreceptor proteins: the cGMP cascade. In *The Molecular Mechanism of Photoreception*, ed. STIEVE, H., pp. 51–66. Dahlem Konferenzen. Berlin: Springer.

BADER, C. R., BERTRAND, D. & SCHWARTZ, E. A. (1985). Voltage-activated and calcium-activated currents studied in solitary rod inner segments from the salamander retina. *Journal of Physiology* **331**, 253–284.

BADER, C. R., MACLEISH, P. R. & SCHWARTZ, E. A. (1979). A voltage-clamp study of the light-response in solitary rods of the tiger salamander. *Journal of Physiology* **296**, 1–26.

BAEHR, W., DEVLIN, M. J. & APPLEBURY, M. L. (1979). Isolation and characterization of cGMP phosphodiesterase from bovine rod outer segments *Journal of Biological Chemistry* **254**, 11669–11677.

BARKDOLL III, A. E., PUGH JR, E. N. & SITARAMAYYA, A. (1986). Hydrolysis of 8-Bromo-cyclic

GMP by the light-activated phosphodiesterase of toad retinal rods. *Biophysical Journal* **49**, 279a.

BAUMANN, C. (1978). The equilibrium between metarhodopsin I and metarhodopsin II in the isolated frog retina. *Journal of Physiology* **279**, 71–80.

BAYLOR, D. A., HODGKIN, A. L. & LAMB, T. D. (1974). The electrical response of turtle cones to flashes and steps of light. *Journal of Physiology* **242**, 685–727.

BAYLOR, D. A. & LAMB, T. D. (1982). Local effects of bleaching in retinal rods of the toad. *Journal of Physiology* **328**, 49–71.

BAYLOR, D. A., LAMB, T. D. & YAU, K.-W. (1979*a*). The membrane current of single rod outer segments. *Journal of Physiology* **288**, 589–611.

BAYLOR, D. A., LAMB, T. D. & YAU, K.-W. (1979*b*). Responses of retinal rods to single photons. *Journal of Physiology* **288**, 613–634.

BAYLOR, D. A., MATTHEWS, G. & NUNN, B. J. (1984). Location and function of voltage-sensitive conductances in retinal rods of the salamander, *Ambystoma tigrinum*. *Journal of Physiology* **354**, 203–223.

BAYLOR, D. A. & NUNN, B. J. (1986). Electrical properties of the light-sensitive conductance of salamander rods. *Journal of Physiology* **371**, 115–145.

BENNETT, N., MICHEL-VILLAZ, M. & KUHN, H. (1982). Light-induced interaction between rhodopsin and the GTP-binding protein: metarhodopsin II is the major photoproduct involved. *European Journal of Biochemistry* **127**, 97–103.

BODOIA, R. D. & DETWILER, P. B. (1984). Patch-clamp recordings of the light-sensitive dark noise in retinal rods from the lizard and frog. *Journal of Physiology* **367**, 183–216.

COBBS, W. H. & PUGH JR, E. N. (1985). Cyclic GMP can increase rod outer-segment light-sensitive current 10-fold without delay of excitation. *Nature* **313**, 585–587.

COREY, D. P. & STEVENS, C. F. (1983). Science and technology of patch-recording. In *Single Channel Recording*, ed. SAKMANN, B. & NEHER, E., chap. 3, pp. 53–68. New York: Plenum.

DARTNALL, H. J. A. (1972). Photosensitivity. In *Handbook of Sensory Physiology*, ed. DARTNALL, H. J. A., vol. VII/4. New York: Springer.

FERSHT, A. (1977). *Enzyme Structure and Mechanism*. San Francisco: Freeman.

FESENKO, E. E., KOLESNIKOV, S. S. & LYUBARSKY, A. L. (1985). Induction by cyclic GMP of cationic conductance in plasma membrane of retinal rod outer segments. *Nature* **313**, 310–313.

FUNG, B. B.-K., HURLEY, J. B. & STRYER, L. (1981). Flow of information in the light-triggered cyclic nucleotide cascade of vision. *Proceedings of the National Academy of Sciences of the U.S.A.* **78**, 152–156.

FUNG, B. B.-K. & STRYER, L. (1980). Photolyzed rhodopsin catalyzes the exchange of GTP for bound GDP in retinal rod outer segments. *Proceedings of the National Academy of Sciences of the U.S.A.* **77**, 2500–2504.

GRAY, P. & ATWELL, D. (1985). Kinetics of light-sensitive channels in vertebrate photoreceptors. *Proceedings of the Royal Society* B **223**, 379–388.

HAYNES, L. W., KAY, A. R. & YAU, K.-W. (1986). Single cGMP-activated channel activity in excised patches of rod outer segment membranes. *Nature* **321**, 66–70.

LAMB, T. D. (1986). Transduction in vertebrate photoreceptors: the roles of cyclic GMP and calcium. *Trends in Neurosciences* **9**, 224–228.

LAMB, T. D., MCNAUGHTON, P. A. & YAU, K.-W. (1981). Spatial spread of activation and background desensitization in toad rod outer segments. *Journal of Physiology* **319**, 463–496.

LIEBMAN, P. A. (1962). In situ microspectrophotometric studies on the pigments of single retinal rods. *Biophysical Journal* **2**, 161–178.

LIEBMAN, P. A. (1972). Microspectrophotometry of photoreceptors. In *Handbook of Sensory Physiology*, ed. DARTNALL, H. J. A., vol. VII/1, pp. 482–525. Berlin: Springer.

LIEBMAN, P. A. & ENTINE, G. (1974). Lateral diffusion of visual pigment in photoreceptor disk membranes. *Science* **185**, 457–459.

LIEBMAN, P. A. & EVANCZUK, A. T. (1982). Real time assay of rod disk membrane cGMP phosphodiesterase and its controller enzymes. *Methods in Enzymology* **81**, 532–542.

LIEBMAN, P. A. & PUGH JR, E. N. (1981). Control of rod disk membrane phosphodiesterase and a model for visual transduction. In *Molecular Mechanisms of Photoreceptor Transduction, Current Topics in Membranes and Transport*, ed. MILLER, W. H., vol. 15, pp. 157–170.

LIEBMAN, P. A. & PUGH JR, E. N. (1982). Gain, speed and sensitivity of GTP binding *vs.* PDE activation in visual excitation. *Vision Research* **22**, 1475–1480.

MATTHEWS, G. (1987). Single-channel recordings from light-sensitive and cGMP-sensitive channels of the rod photoreceptors. *Proceedings of the National Academy of Sciences of the U.S.A.* **84**, 299–302.

PENN, R. D. & HAGINS, W. A. (1972). Kinetics of the photocurrent of retinal rods. *Biophysical Journal* **12**, 1073–1094.

PARKES, J. H. & LIEBMAN, P. A. (1982). pH dependence of light-sensitive PDE activation matches fraction of bleached rhodopsin converted to metarhodopsin II. *Investigative Ophthalmology and Visual Science* **22**, 44a.

POO, M. M. & CONE, R. A. (1974). Lateral diffusion of rhodopsin in photoreceptor membranes. *Nature* **247**, 438–441.

PUGH JR, E. N. & COBBS, W. H. (1986). Visual transduction in vertebrate rods and cones: a tale of two transmitters, calcium and cyclic GMP. *Vision Research* **26**, 1613–1643.

RAE, J. & LEVIS, R. A. (1984). Patch clamp recording from the epithelium of the lens obtained using glasses selected for low noise and improved sealing properties. *Biophysical Journal* **45**, 144–146.

STRYER, L. (1986). The cyclic GMP cascade of vision. *Annual Review of Neuroscience* **9**, 87–119.

SZABO, A., SCHULTEN, K. & SCHULTEN, Z. (1980). First passage time approach to diffusion-controlled reactions. *Journal of Chemical Physics* **72**, 4350–4357.

VUONG, T. M. & STRYER, L. (1984). Millisecond activiation of transducin in the cyclic nucleotide cascade of vision. *Nature* **311**, 659–661.

YAU, K.-W. & NAKATANI, K. (1984). Electrogenic Na/Ca exchange in retinal rod outer segments. *Nature* **311**, 661–663.

YAU, K.-W. & NAKATANI, K. (1985*a*). Light-induced reduction of cytoplasmic free calcium in retinal rod outer segments. *Nature* **313**, 579–581.

YAU, K.-W. & NAKATANI, K. (1985*b*). Light-suppressible, cGMP-sensitive conductance in the plasma membrane of a truncated rod outer segment. *Nature* **317**, 252–255.

ZIMMERMAN, A. L. & BAYLOR, D. A. (1986). Cyclic GMP-sensitive conductance of retinal rods consists of aqueous pores. *Nature* **321**, 70–72.

ZIMMERMAN, A. L., YAMANAKA, G., ECKSTEIN, F., BAYLOR, D. A. & STRYER, L. (1985). Interaction of hydrolysis-resistant analogs of cyclic GMP with the phosphodiesterase and light-sensitive channel of retinal rod outer segments. *Proceedings of the National Academy of Sciences of the U.S.A.* **82**, 8813–8817.